Source Mergers and Bubble Growth During Reionization

J.D. Cohn*[a,b] and Tzu-Ching Chang†[b]
[a] *Space Sciences Laboratory,*
[b] *Theoretical Astrophysics Center, Dept. of Astronomy, University of California, Berkeley, CA 94720*

February 5, 2008

Abstract

The recently introduced models of reionization bubbles based on extended Press-Schechter theory (Furlanetto, Zaldarriaga & Hernquist (2004a)) are generalized to include mergers of ionization sources. Sources with a recent major merger are taken to have enhanced photon production due to star formation, and accretion onto a central black hole if a black hole is present. This produces a scatter in the number of ionized photons corresponding to a halo of a given mass and a change in photon production over time for any given halo mass. By extending previous methods, photon production histories, bubble distributions, and ionization histories are computed for several different parameter and recombination assumptions. The resulting distributions interpolate between previously calculated limiting cases.

1 Introduction and Background

Reionization marks the historical event when hydrogen in the universe transformed from mostly neutral to mostly ionized; it has only recently become accessible via observations and numerical simulations and has stirred great interest and advances in our understanding of early structure formation (see e.g. reviews by Barkana & Loeb (2001), Loeb & Barkana (2001), Cooray & Barton (2006), Loeb (2006)).

Current observations suggest that the process of reionization is complex, perhaps lasting over an extended period of time (for a review, see Fan, Carilli

*jcohn@berkeley.edu
†tchang@astron.berkeley.edu

& Keating (2006)). The optical depth to electron scattering seen by WMAP (Spergel et al (2006)) can be modeled with reionization starting by $z \geq 10$. On the other hand, spectroscopic observations of high-redshift quasars find Gunn-Peterson absorption due to intervening neutral hydrogen in the intergalactic medium (Becker et al (2001), Fan et al (2003),White et al (2005)), although with significant fluctuations along different lines of sight (Oh & Furlanetto (2005)), which suggests that the tail end of reionization occurs at $z \sim 6$.

Theoretically, questions about reionization range from the fundamental timeline of reionization to detailed characteristics. The latter include the nature of ionizing sources, the topology of the ionized regions and their evolution, and the behavior of the ionized regions relative to matter overdensities and voids. Numerical approaches (e.g. Gnedin (2000), Razoumov et al (2002), Ciardi, Stoehr & White (2003), Sokasian et al (2003; 2004)) are fruitful due to the complex nature of the sources and nonlinear clustering involved. For small regions, simulations can track the nonlinear effects, although much known physics is too difficult to incorporate, and much unknown physics remains. However, the large disparity in size between the ionized regions (which can grow to be tens of Mpc comoving, e.g. Wyithe & Loeb (2004), Furlanetto, Zaldarriaga & Hernquist (2004a)) and the small scale distributions and physics of sources producing the photons is difficult to capture in a simulation. Recent numerical simulations have just begun to combine large and small scale effects in larger volumes (see for instance Kohler, Gnedin & Hamilton (2005), Iliev et al (2005)).

Analytic models are useful to encompass the wide range of scales in order to try to identify generic behavior. In addition, analytic models allow exploring a larger range of parameters and other assumptions. This paper extends an analytic model introduced by Furlanetto, Zaldariagga and Hernquist (2004a) (hereafter FZH) to characterize the growth of ionized regions or bubbles. The basic idea is to move beyond the initial step of considering HII regions around individual collapsed halos (e.g. Arons & Wingert (1972), Barkana & Loeb (2001)) to consider regions around several collapsed halos. The simplest form goes as follows: collapsed halos of mass m are able to ionize a mass M where

$$M = \zeta m \tag{1}$$

and ζ is a constant. Halos need to be massive enough to produce photons, thus $m > m_{min}(z) = m(T = 10^4 K, z)$ is imposed, i.e. they need to be massive enough to have efficient atomic Hydrogen line cooling. For a constant ζ, independent of m, the size of ionized regions can be calculated immediately in closed form: an ionized region of mass M has the fraction of mass f_{coll} bound in halos above $m_{min}(z)$ equal to or greater than ζ^{-1}. Using extended Press-Schechter theory (references below), the mass fraction f_{coll} in a fully

ionized bubble of mass M then obeys

$$f_{coll} = \mathrm{erfc}[\frac{\delta_c(t) - \delta_M}{\sqrt{2(\sigma^2_{min} - \sigma^2(M))}}] > \zeta^{-1} \ . \tag{2}$$

This constrains the average overdensity δ_M for any M. Here σ_{min} denotes the density fluctuations smoothed on a scale of mass $m_{min}(z)$, likewise for $\sigma^2(M)$, and $\delta_c(t)$ is the threshhold density for collapse. The overdensity required for collapse is $\delta_c = 1.686$, in this picture the densities stay constant and the threshold lowers with time, so $\delta_c(t) = \delta_c/D(z(t))$ where $D(z)$ is the growth factor. The bubble's average overdensity relative to $\delta_c(t)$ is δ_M, corresponding to physical overdensity $\delta_{R,M}(t) = \delta_M D(z(t))$, and $V_M(1 + \delta_{R,M}(t))\bar{\rho} = M$, where V_M is the bubble volume and $\bar{\rho}$ is the mean density. The condition for a bubble to be ionized, equation 2, can be rewritten in a form that is more easily generalizable,

$$\zeta f_{coll} = 1 \ . \tag{3}$$

The function δ_M allows one to determine the number distribution of bubbles of mass M and other properties discussed below.

In FZH, recombinations were included implicitly in ζ. A more sophisticated approach balancing the total number of ionizations and recombinations per unit time in the intergalactic medium (IGM) was introduced in Furlanetto & Oh (2005) (hereafter FO05), where they considered two models of IGM gas density distribution for recombinations: one model adopted an analytical fit of gas density to simulations at low redshift by Miralda-Escude, Haehnelt & Rees (2000), and extrapolated it to high z; a second model considered minihalos as photon sinks. Minihalos are neutral, dense blobs with mass $10^6 M_\odot$, randomly distributed in the IGM.

These results were extended by Furlanetto, McQuinn & Hernquist (2005) (hereafter FMH05) and others. For example, FMH05 include the effects of different halo mass functions, a mass dependent $\zeta(m)$, and stochastic fluctuations in the galaxy distribution. They found the consequences of these additional effects on the bubble size distributions and corresponding evolution in time, the emissivity inside a bubble, the observable neutral hydrogen 21 cm power spectra, and the kinetic Sunyaev-Zel'dovich signal. Tools for calculations of the latter were developed by Zahn et al (2005) and McQuinn et al (2005a), they also extended many aspects of the approach. Other consequences of this model for observables have been calculated, for example in Furlanetto, Hernquist & Zaldarriaga (2004), Furlanetto, Zaldarriaga & Hernquist (2004b; 2006), McQuinn et al (2005b) and Alvarez et al (2005).

Here we extend this model further to include the effects of major mergers. The original models are based on a time independent ζ which only depends upon mass. Halos which have recently had a major merger produce an increased number of photons, due to starbursts (1:3 halo mass ratios) or

induced black hole accretion (1:10 halo mass ratios). Consequently major mergers introduce a time dependence in the average of ζ and a scatter in ζ. We expect halo major mergers to be important, as even the smallest objects producing photons (chosen to be those with $T > 10^4 K$) have masses several orders of magnitude above M_* at high redshifts, and thus are highly biased and very actively merging.[1] We use estimates of photon production due to quiescent star formation, merger induced starbursts and black hole accretion. As the photon production estimates have many unknowns, we are especially interested in features which characterize the merging itself rather than the details we choose.[2]

There are several related studies in this active area of research. This is not the mergers of the bubbles, which was already considered in FO05. The scatter discussed is not the scatter (Furlanetto et al (2005)) in ζ due to the stochasticity of the number of collapsed halos (Barkana & Loeb (2004a), Babich & Loeb (2005)), or the difference between metal rich and metal poor regions (Barkana & Loeb (2005)). Other related work includes the calculation of the effects of mergers in producing cumulative number of photons by quasars up to redshifts ~ 5, e.g. by Wyithe & Loeb (2002) and Madau et al (2004). Here we want the effects of the mergers in producing a time dependent photon production rate, with scatter, for collapsed halos of a given mass, and the consequences for the enclosing bubbles.

Section §2 gives the analytic framework and formulae for the merger rates, recombinations and scatter. The natural quantity to use is the instantaneous photon production rate which then determines the time derivative of ζ_t rather than ζ itself. The resulting formalism is a natural extension of earlier work (e.g. FZH04, FO05, FMH05): their early time limit took reionization to only depend on the halos present at the time under consideration and included recombinations implicitly, the late time limit imposed equilibrium between instantaneous photon production and recombination rates. The extension of these earlier formalisms, introduced here, finds the total number of ions present by integrating the photon production rate over time (due to the halos present at any instant), and subtracting recombinations. Three prescriptions for recombinations are used. The scatter requires additional assumptions, we describe and choose a simple case next. In section §3, we calculate the analytic form of the time derivative ζ_t in terms of the star formation and black hole accretion parameters and then explicitly show its dependence upon

[1] M_*, a function of time, is the mass at which $\sigma(M) = \delta_c(t)$. An estimate of the formation minus destruction rate for halos of mass M is proportional to $\delta_c(t)/\sigma^2(M) - 1/\delta_c(t)$, see e.g. Kitayama & Suto (1996). For $M > M_*$ this rapidly increases with M and can be thought of as indicative of not only a high formation rate but also a high major merger rate–more detailed calculations confirm this trend.

[2] Ideally this could eventually be turned around to constrain assumptions going into the photon production estimates but it is not clear how constraining that might be given the vast uncertainties.

mass and redshift for a few examples. Section §4 shows the effects on bubbles using a fiducial model and some variations: the bubble overdensity δ_M as a function of bubble mass M (as a function of redshift and initial conditions), the characteristic bubble sizes and ionization fractions over time $\bar{x}_i$, and the bubble size distributions associated with the (major) merger scatter. Section §5 concludes. An appendix spells out the basic Extended Press- Schechter quantities, details the estimates used to find the minimum halo mass for a black hole to be present and describes some other possible assumptions for scatter. The term ionized mass fraction refers to the mass found in ionized bubbles unless otherwise stated.

2 Analytic Framework

In this section we describe the analytic calculations, assumptions and formulae used in the rest of the paper: the halo mass function, major merger rates, recombinations and the merger related scatter. The input parameters to most of our calculations are $\Omega_m = 0.3, \Omega_\Lambda = 0.7, \sigma_8 = 0.9, \Omega_b h^2 = 0.02, h = 0.7$ a scale invariant initial power spectrum $n = 1$, and the Eisenstein-Hu (1997) transfer function. Our fiducial model has these parameters. We considered several changes of cosmology. We used the above and only changed n to 1.05, which enhances fluctuations for large k, i.e. small scales, and we fixed to the above but instead took $\Omega_b h^2 = 0.225$. Another variant we considered was the set of parameters from the recent WMAP analysis (Spergel et al (2006)): $\Omega_m = 0.24, \Omega_\Lambda = 0.7, \sigma_8 = 0.74, \Omega_b h^2 = 0.0223, h = 0.73$, we discuss these at the end. Masses are defined in terms of $h^{-1} M_\odot$ and all lengths are comoving.

2.1 Halo Mass Function

The starting point for the extended Press-Schechter bubble model of reionization is the number density of collapsed halos of dark matter. We use the Press-Schechter formalism (1974) to estimate numbers and source major merger rates. Examples of the resulting number densities and properties have been detailed by Barkana & Loeb (2001) and Mo & White (2002).

Our use of the Press-Schechter mass function warrants some discussion. The Sheth-Tormen (2002) mass function is a better fit to simulations at low redshifts; mass functions found in high redshift simulations (Jang-Condell & Hernquist (2001), Reed et al (2003), Heitmann et al (2006), Iliev et al (2005)) often lie between Sheth-Tormen and Press-Schechter (the best agreement for Heitmann et al was with the fitting function of Warren et al (2005)). Agreement with dark matter simulations is not necessarily indicative of appropriateness either, as baryons and dark matter are not as tightly coupled at high redshifts (e.g. Naoz & Barkana (2005), Bagla & Prayad (2006)). For

the original model (which we modify here), the the effect of using the Sheth-Tormen mass function instead of the Press-Schechter mass function for the number of sources was seen to be small (Furlanetto et al (2005)). We altered the "tilt" n in one set of runs from $n = 1$ to $n = 1.05$ to see the effect of increased small scale structure as found in these simulations.

The Press-Schechter mass function is the most tractable and our interest is in trends rather than exact numbers. With it, the number of recently merged halos can be calculated easily using extended Press Schechter theory (Bond et al (1991), Lacey & Cole (1993; 1994), Bower(1991), Kitayama & Suto (1996)).[3] There are problems as well with extended Press-Schechter theory, especially when considering large mass ratios in merger rates (see Benson et al (2005) for a recent discussion of this). We restrict ourselves to major mergers, with small mass ratios. In addition to being in the regime where extended Press-Schechter works the best, this allows predecessors and final halos to be identified uniquely (a halo only has one predecessor with mass greater than half the final halo mass).

2.2 Photon Sources

2.2.1 Major Merger Rates

After a major merger, a halo produces extra photons for some specified amount of time, denoted t_{ion}. We are interested in the number of halos of a given mass which are still "active," i.e. which are still producing extra photons due to a recent major merger. We ignore the lag between the actual merger and the beginning of the photon production, which should not change the general trends of interest. We also assume that the extra photon production rate is constant during t_{ion} after the merger, so that we do not care about when exactly the merger happened, only that it happened within this relaxation time.

The number of recently merged halos with mass m at time t is the product of two factors, depending upon two times: the time of the merger t_i and the subsequent time of observation t, where the latter is close enough to t_i for the halo to still be excited from the merger, i.e. $t - t_i < t_{ion}$. The first factor is the fraction of halos that have mass m_0 which have jumped at time t_i from mass m_i, $\dot{P}_1(m_i \rightarrow m_0; t_i)\frac{m_0}{m_i} dm_i dt_i$. (The overdot denotes derivative with respect to t_i.) The factor of m_0/m_i makes the conversion from the number of points coming from m_i halos (the quantity given by the formalism) to the total number of points in their descendant m_0 halos.[4] We then want

[3] These are actually formulae for fast mass gain and can include accretion. Analytic formulae differentiating between major mergers and accretion have been found by Raig et al (1998), Salvador-Sole et al (1998) and Andreu et al (2001).

[4] If the m_0 halo has come from an m_i halo, all of its mass was not previously in the m_i halo, only m_i/m_0 of its mass. But the quantity wanted here is the full mass of halos which

this "excited" halo of mass m_0 to be in a halo of mass m at time t. The probability that a point in a halo of mass m at time t was in a halo of mass m_0 at time t_i is $P_1(m_0, t_i|m, t)dm_0$. Formulae for P_1 and its derivative are in the appendix.

For bubbles we need to go one step further and consider the regions of mass M surrounding these mass m sources. The probability that a halo (bubble) of mass M and overdensity δ_M contains a halo of mass m at time t is denoted by $P_1(m, t|M, \delta_M)dm$, corresponding to a number density of halos $n(m, t|M, \delta_M)dm = \frac{\bar{\rho}}{m}P_1(m, t|M, \delta_M)dm$. (When a time t rather than δ is written as an argument of P_1 the implicit assumption is that one uses $\delta_c(t)$ in P_1, the threshold density corresponding to time t.) Thus the number of halos which have merged at time t_i from mass m_i to mass m_0 and are in a halo of mass m at time t within a bigger halo (bubble) of mass M and overdensity δ_M is given by (see Appendix for more discussion and details):

$$V_M n(m, t|M, \delta_M)\dot{P}_1(m_i \to m_0, t_i)P_1(m_0, t_i|m, t)\frac{m}{m_i}dmdt_i dm_i dm_0 \ . \qquad (4)$$

2.2.2 Total Photon Rates

The rate photons are produced in a region with mass M and overdensity δ_M is the number of additional photons due to the mergers, plus the quiescent number of photons due to the collapsed halos present even if no merger has occurred. (We assume that each photon produced corresponds to an ionization in the region, in principle the bubble region can have some "escape fraction" which would effectively lower the number of ionizations in a region relative to the number of photons produced.) A constant ζ for sources of lifetime ΔT gives a $\zeta_t = \zeta/\Delta T$. More generally, there is a dependence upon the mass of the initial and final masses before the merger (m_i, m_0), the mass m at the time of interest, and t_i, t to give $\zeta_t(m_i, m_0, t_i, m, t)$. The quiescent rate is taken to be $\zeta_{t,q}(m)$. These quiescent photons are from stars not created during starbursts, i.e. ongoing star formation, in part due to accretion. Putting this together to get the rate mass is ionized gives

$$\begin{aligned}
&\int dmn(m, t|M, \delta_M)\tfrac{m}{\bar{\rho}} \\
&\{\int dt_i dm_i dm_0 \zeta_t(m_i, m_0, t_i, m, t)\dot{P}_1(m_i \to m_0, t_i)P_1(m_0, t_i|m, t)\tfrac{m}{m_i} + \zeta_{t,q}(m)\} \\
&= \int dmn(m, t|M, \delta_M)\tfrac{m}{\bar{\rho}}\zeta_{t,a}(m) \\
&= (\zeta f)_t
\end{aligned} \qquad (5)$$

The above defines $(\zeta f)_t$ and $\zeta_{t,a}(m)$. Section §3 derives estimates for $\zeta_t(m_i, m_0, t_i, m, t)$ using models for star formation and black hole accretion,

have had mergers, i.e. halos which now have mass m_0 but had such an m_i component earlier; thus the factor m_0/m_i is included.

and gives parameters and limits for the integrals. In the integrals, the mass limits are determined by the mass ratio criteria for major mergers. In all cases we require $m_{i,max}/m_0 > m_i/m_0 > 0.5$. The lower limit means some major mergers are neglected, but ensures that no major merger is counted twice, as only one halo with $m_i > m_0/2$ can end up in m_0. This is thus a lower limit on the number of mergers. The time limits in the integrals are determined by the time scales of relaxation after the mergers. Both the mass and time limits can differ for starbursts and black hole accretion.

In principle $m_{0,min}$ can be as small as $m(T = 10^4K, z) = \frac{2.04\times10^9}{(1+z)^{3/2}}h^{-1}M_\odot$. However the probabilities above double count a halo which has two mergers within a relaxation time, which is more likely if $m_{0,min}$ is chosen to be small. For the number of photons contributed, this is perhaps accurate (but perhaps not, e.g. for starbursts there might be gas missing after the first merger for some period of time). However for the scatter it will give two final halos with recent mergers rather than just the one which had two mergers. However, if $m_{0,min}$ is taken to be too large, the number of photons will be undercounted and the scatter underestimated. We used both $m_{0,min} = 0.1m$ and $m_{0,min} = m_{min}(T = 10^4K, z)$ in our calculations,[5] for nontrivial mass dependence of star formation (referred to as $\alpha = 2/3$ below) these two choices are essentially indistinguishable.

The ionized mass fraction in a region of mass M with overdensity δ_M, the generalization of equation 3, is then

$$\int dt[(\zeta f)_t - R_{recomb}(R_{ion}(M), \delta_M, t)] \; . \tag{9}$$

where $R_{recomb}(t)$ is the instantaneous recombination rate in the bubble volume, depending upon $R_{ion}(t)$, the effective radius of the ionized region at this time. The dependence upon R_{ion} takes into account that not all regions inside a bubble at time t are ionized at earlier times: recombinations can only occur where there are ions already present. As the first term gives the total number of photons produced in the region, assumed to produce the same number of ions, recombinations can be directly subtracted off.

[5]If we take the limits of m_0 to be independent of m, then the integral over m can be done explicitly using an identity for composing the probabilities. This gives the mass fraction which had mergers at t_i to mass m_0 in a halo of mass M as

$$\int dm\dot{P}_1(m_i \to m_0; t_i)\frac{m}{m_i}P_1(m_0, t_i|m, t)P_1(m, t|M, \delta_M)dm_i dm_0 dt_i \tag{6}$$

$$= \dot{P}_1(m_i \to m_0; t_i)\frac{m}{m_i}P_1(m_0, t_i|M, \delta_M)dm_i dm_0 dt_i \tag{7}$$

$$\tag{8}$$

i.e. it doesn't matter what m halo the original m_0 halo is in at time t, just that it is in the bubble M.

2.3 Recombination

Recombinations decrease the number of ions present. We use the two estimates for the recombination rate for an ionized region of radius $R_{ion}(t)$ and overdensity δ_M chosen by FO05 and a third by Mellima et al (2006). The recombination rate per hydrogen atom inside an ionized region of radius R_{ion} at time t and overdensity δ_M is

$$\alpha_A(T) n_e C(R_{ion}(t)) = A_u(1+\delta_{R,M}(t))C(R_{ion}(t)) \ , \tag{10}$$

where $n_e = \bar{n}_e(1+\delta_{R,M}(t))$. The physical overdensity $\delta_{R,M}(t)$ enhances the rate at mean density $A_u = \alpha_A(T)\bar{n}_e = 2.4 \times 10^6/Myr$. (We use $\alpha_A(T = 10^4 K)$ for case A recombination, case B recombination (optically thick) takes $A_u \rightarrow 0.6A_u$.) The three recombination models have different clumping factors, described in subsections below.

To go from the ionization rates per hydrogen atom in the bubble to the change in ionization fraction in equation 9 requires the comparison of counts[6]: counts of ions present and counts of recombinations depleting ions. The ionized mass fraction times the hydrogen mass of the bubble gives the number of ions in the bubble at a given time. The recombination rate at the same time is the rate per hydrogen atom times the number of ionized hydrogen atoms, $\bar{n}_h(1+\delta_{R,M}(t))V_{ion}$. Here V_{ion} is the volume of the region where the hydrogen is ionized and M_{ion} is its mass. Dividing by the total mass of the bubble and noting $V_{ion} = \frac{M_{ion}}{M}\frac{M}{(1+\delta_{R,M}(t))\bar{\rho}}$, the resulting ionization fraction with recombinations included, at some time t, is

$$\int^t dt'[(\zeta f)_{t'} - A_u \frac{M_{ion}(t')}{M}(1+\delta_{R,M}(t'))C(R_{ion}(t'))] \ . \tag{11}$$

The mechanics of doing this integral are discussed in section §4, we now describe the clumping factors $C(R_{ion})$ for the three different recombination models.

2.3.1 The MHR model

The first model (hereafter called the MHR model) is a smooth IGM gas distribution of Miralda-Escude, Haehnelt & Rees (2000). They use the volume density distribution of IGM gas, $P_V(\Delta)$ ($\Delta = \rho/\bar{\rho}$) fit to simulations at $z \sim 2-4$, finding

$$P_V(\Delta)d\Delta = A_0 \Delta^{-\beta} \exp[-\frac{(\Delta^{-2/3} - C_0)^2}{2(2\delta_0/3)^2}]d\Delta \tag{12}$$

with $\beta = 2.5$. A_0 and C_0 are set by requiring mass and volume normalization and δ_0 is the variance of density fluctuations smoothed on the Jeans scale for

[6]We thank S. Furlanetto for discussions about this.

an ionized medium (at higher z, $\delta_0 = 7.61/(1+z)$ to better than 1%). The distribution $P_V(\Delta)$ is taken to be independent of environment (rather than depending upon δ_M). For recombination, they assume all gas below some density threshold $\Delta < \Delta_i$ is ionized and everything above is shielded. One finds Δ_i by noting that recombination limits bubble growth– i.e. the mean free path $\lambda_i = \lambda_0[1 - F_V(\Delta_i)]^{-2/3}$ is the radius of the ionized region R_{ion}. Here $\lambda_0 H(z) = 60\mathrm{km\ s^{-1}}$ (in physical units) and $F_V(\Delta_i)$ is the fraction of volume with $\Delta < \Delta_i$. (If the region's radius $R_{ion} < \lambda_0$ then the assumption is that recombination is negligible and Δ_i is set to zero.) The factor C is then

$$C_{MHR}(R_{ion}) = \int_0^{\Delta_i} d\Delta P_V(\Delta)\Delta^2 \ , \tag{13}$$

again, note R_{ion} enters implicitly via $\Delta_i(R_{ion})$. At large R_{ion} $C_{MHR}(R_{ion})$ tends to asymptote to a constant, and for most (all) radii it is smaller than $C_{mh}(R_{ion})$ (C_{MIPS}) described below.

2.3.2 Minihalos

The second model is a minihalo model (FO05) of small dense absorbing clumps, taken to have mass of $M_{mh} = 10^6 M_\odot$ with comoving mean free path

$$\begin{aligned} \ell_{mh} &= \tfrac{1}{\pi n_{mh} R_{mh}^2} \\ &\sim 15.7h(\tfrac{M_{mh}}{10^6 M_\odot})^{1/3}(\tfrac{0.05}{f_{mh}})(\tfrac{\Delta_{mh}}{18\pi^2})^{2/3}(\tfrac{\Omega_m h^2}{0.15})^{-1/3}\mathrm{h^{-1}\ Mpc} \end{aligned} \tag{14}$$

and

$$C_{mh}(R_{ion}) = (1 - f_{mh})^2 \exp(R_{ion}/\ell_{mh}) \tag{15}$$

where $f_{mh} = 0.05$ is the mass fraction taken to be in minihalos. Unlike the other two models it is redshift independent. Note that the effect of minihalos on recombination and thus reionization is likely to be more complicated than this simple prescription, which is probably an overestimate (Iliev, Scannapieco & Shapiro (2005), Ciardi et al (2006)).

2.3.3 The MIPS model

A third prescription from clumping, matched to numerical simulations is by Mellema, Iliev, Pen & Shapiro (2006) (MIPS), which is an improved fit for the IGM clumping factor to the one given by Iliev et al (2005). They used a N-body simulation with a 3.5 h^{-1} Mpc box and 3248^3 particles to get a mass resolution down to the Jeans mass; they then took out all found halos, including minihalos, to eliminate their contributions to the IGM density field. The resulting IGM was fit to give an R_{ion} independent clumping factor:

$$C_{MIPS} = 27.466 \exp(-0.114z + 0.001328z^2) \tag{16}$$

It resembles the MHR clumping factor at large R_{ion} as the former asymptotes to a constant for large R_{ion} and high z, but is larger numerically, and thus more effective at suppressing bubble formation than the MHR model. This will be referred to as the MIPS model in the following.

2.4 Scatter

Extended Press-Schechter gives the fraction of halos which have had recent mergers. This is an average quantity, just as the number of collapsed halos in a larger region of mass M is given only on the average by $n(m, t|M, \delta_M)$. In any region a scatter in the number of sources will lead to a scatter the number of ionizing photons and thus in bubble sizes. For $n(m, t|M, \delta_M)$, FMH05 took the scatter due to the stochastic nature of the collapsed halo distribution (halos of mass m) in the larger bubbles of mass M to be Poisson. Numerical simulations have found this scatter to be within a factor of two of Poisson for the cases studied by Sheth & Lemson (1999) and Casa-Miranda et al (2002). In equations, the ionized mass fraction is

$$\int dm\zeta(m)\frac{m}{\bar{\rho}}n(m, t|M, \delta_M) \tag{17}$$

and they assumed for the scatter

$$\begin{aligned}\langle n(m, t|M, \delta_M)n(m', t|M, \delta_M)\rangle &= n(m, t|M, \delta_M)n(m', t|M, \delta_M) \\ &\quad +\tfrac{\delta_D(m-m')}{V_M}n(m, t|M, \delta_M)\ .\end{aligned} \tag{18}$$

where δ_D is a Dirac delta function.

For our case we want the scatter of

$$\int dt \int dmn(m, t|M, \delta_M)\frac{m}{\bar{\rho}}\zeta_{t,a}(m)\ ; \tag{19}$$

i.e.

$$\int dtdt'dmdm'\frac{mm'}{\bar{\rho}^2}\langle n(m, t|M, \delta_M)\zeta_{t,a}(m)n(m', t'|M, \delta_M)\zeta_{t',a}(m')\rangle\ ; \tag{20}$$

Thus instead of the scatter of $n(m, t|M, \delta_M)$ for fixed time above, we need

$$\langle n(m, t|M, \delta_M)n(m', t|M, \delta_M)\rangle\ . \tag{21}$$

In addition, $\zeta_{t,a}(m)$ has scatter. To our knowledge the appropriate distributions have not been calculated in numerical simulations, and thus additional assumptions are required to continue.

The simplest assumption is to take the distribution of $n(m, t|M, \delta_M)$ to be Poisson both in mass and in time:

$$\begin{aligned}\langle n(m, t|M, \delta_M)n(m', t'|M, \delta_M)\rangle &= n(m, t|M, \delta_M)n(m', t'|M, \delta_M) \\ &\quad +\tfrac{1}{V_M}\delta_D(m-m')\delta_D(\delta(t)-\delta(t'))n(m, t|M, \delta_M)\end{aligned} \tag{22}$$

Note that n is a function of t only through $\delta(t)$ and thus $\delta(t)$ is taken to be the argument of the Dirac delta function. Using $\delta_D(t-t')$ would give the wrong dimensions.

The second assumption is for the scatter of

$$\zeta_{t,a}(m) = \int dt_i dm_i dm_0 \zeta_t(m_i, m_0, t_i, m, t) \dot{P}_1(m_i \to m_0, t_i) P_1(m_0, t_i|m, t) \frac{m}{m_i} + \zeta_{t,q}(m) \ . \tag{23}$$

We define $n^a(m_0|m,t)$ which appears in $\zeta_{t,a}(m)$ the following way:

$$\int dt_i dm_i \zeta_t(m_i, m_0, t_i, m, t) \dot{P}_1(m_i \to m_0, t_i) \frac{m_0}{m_i} P_1(m_0, t_i|m, t) = \sum_{a=1}^{3} \frac{m_0}{\bar{\rho}} n^a(m_0|m,t) \zeta_t^a(m_0) \ . \tag{24}$$

The number density $n^a(m_0|m,t)$ counts the recently merged halos of mass m_0 in a halo of mass m, with the index a denoting the range of integration for m_i, t_i. There are three ranges, corresponding to starbursts, black hole accretion or both. For each a, $\zeta_t(m_i, m_0, t_i, m, t)$ only depends on which of these three cases is at hand and the values of m_0, m, and so it is denoted $\zeta_t^a(m_0)$. Values for $m\zeta_t^a(m_0)$ are derived in the section 3.3 and displayed in Table 1 for the starburst and black hole accretion case (the sum of these is needed when both are present). The Poisson assumption for $n^a(m_0|m,t)$ is then

$$\langle n^a(m_0|m,t) n^b(m_0'|m,t) \rangle = \frac{\delta(m_0 - m_0')}{V_m} \delta^{ab} n^a(m_0|m,t) \tag{25}$$

There is also an assumption being made that the number with scatter is related to the product of $\dot{P}_1 P_1$, rather than a separate scatter for the merger rate to mass m_0 and then scatter for the inclusion of these m_0 halos in m.

The full scatter is then

$$\begin{aligned}
&\langle \zeta_{t,a}(m) n(m,t|M,\delta_M) \zeta_{t',a}(m') n(m',t'|M,\delta_M) \rangle \\
&= \zeta_{t,a}(m) n(m,t|M,\delta_M) \zeta_{t',a}(m') n(m',t'|M,\delta_M) \\
&+ \tfrac{1}{V_M} \delta_D(m-m') \delta_D(\delta(t) - \delta(t')) n(m,t|M,\delta_M) \langle \zeta_{t,a}^2(m) \rangle \\
&= \zeta_{t,a}(m) n(m,t|M,\delta_M) \zeta_{t',a}(m') n(m',t'|M,\delta_M) \\
&+ \tfrac{1}{V_M} \delta_D(m-m') \delta_D(\delta(t) - \delta(t')) n(m,t|M,\delta_M) \{ \zeta_{t,a}^2(m) \\
&+ \textstyle\int dm_0 dm_i dt_i (1 + \delta_R(t,t_i)) (\zeta_t(m_i, m_0, t_i, m, t) m)^2 \frac{1}{m m_i} \dot{P}_1(m_i \to m_0, t_i) P_1(m_0, t_i|m,t) \}
\end{aligned} \tag{26}$$

Here $m = (1 + \delta_R(t,t_i)) \bar{\rho} V_m$ was used, where $\delta_R(t,t_i)$ is the physical overdensity $\delta(t) D(z(t_i))$ and the combination $\zeta_t(m_i, m_0, t_i, m, t) m$ was pulled out.

We then define the scatter in $\int dt (\zeta f)_t$ via

$$\Delta(\int (\zeta f)_t dt)^2 = \langle \int dt dt' (\zeta f)_t (\zeta f)_{t'} \rangle - \langle \int dt (\zeta f)_t \rangle \langle \int dt' (\zeta f)_{t'} \rangle \tag{27}$$

We calculated the consequences of this simplest set of assumptions for our models; some other possibilities are described in the appendix.

The scatter is an integral over time. In practice we cannot integrate back to arbitrarily early times, and so an initial condition and initial scatter are needed. See below for discussion.

3 Photon increase from mergers

The analytic expressions above require estimates of $\zeta_t(m_i, m_0, t_i, m, t)$ and the quiescent rate $\zeta_{t,q}(m)$ to give concrete results. The two main sources of extra photons due to a major merger are starbursts and, if a central black hole is present, accretion onto a central black hole (Kauffmann & Haehnelt (2000), Cavaliere & Vittorini (2000)). Merger induced star formation and black hole accretion at high redshift might differ from their low redshift counterparts, detailed calculations and simulations have not yet been done. We use low redshift calculations and measurements as a guide. We stress that we are most interested in the effects of the time dependence, as the unknowns of the detailed modeling are vast.

A major merger to a halo of mass m will add a total number of photons $N_\gamma(m)$ over a time t_{ion}. These N_γ photons can ionize the hydrogen in a region with mass M obeying $N_\gamma = \frac{M}{m_p}\frac{\Omega_b X}{\Omega_m}$ where $X = 0.76$ and m_p is the proton mass.[7] This is the amount of mass M that can be ionized over the whole time T, giving, if $M = \zeta m$,

$$\zeta = \frac{N_\gamma}{m}\frac{m_p}{X}(\frac{\Omega_b}{\Omega_m})^{-1} \tag{28}$$

We will want to compare the contributions to photons at some given time, thus we will look at all the photons being contributed assuming a constant[8] production rate, i.e. $\zeta_t = \frac{\zeta}{t_{ion}}$. The times t_{ion} for black hole accretion and starbursts differ in general.

3.1 Star Formation and Starbursts

Photon production due to star formation can be estimated via (e.g. Loeb, Barkana & Hernquist (2005))

$$\frac{dN_\gamma, stars}{dt} = \frac{m}{m_p}\frac{\Omega_b}{\Omega_m}\frac{N_{ion}}{t_*} \ . \tag{29}$$

[7] In practice there will be a small correction, perhaps of order 10% due to the possibility that some of the photons will ionize Helium instead, which should be kept in mind. It can be thought of as a rescaling of our fiducial input parameters. We thank the referee for pointing this out.

[8] More accurately, the accretion onto a black hole, if Eddington as is commonly assumed, tends to increase with time until all the infalling material is gone, while the starbursts tend to decay with time until all the gas is gone. However other estimates of black hole accretion have the accretion also slow down with time as the gas supply is decreased.

leading to

$$\zeta_t(m_i, m_0, t_i, m, t) = \frac{1}{X}\frac{N_{ion}}{t_*}\ (stars) \tag{30}$$

Here N_{ion} is the overall number of ionizing photons per baryon in the halo. We assume that the starbursts change the rate from a constant quiescent rate to a constant starburst rate for a time $t_* + t_{burst}$, until the stars due to the starburst are gone.[9]

For N_{ion} our parameters are similar to Loeb et al (2005). We take a star lifetime $t_* = 80Myr$. Showing our choices in parentheses[10], the efficiency with which baryons are incorporated into stars is $f_*(=0.1)$, and each baryon in a star produces $N_{\gamma,bary}(=4400)$ photons, with $f_{esc}(=0.05)$ of them escaping. Combining these we get

$$\begin{array}{ll} N_{ion} & = N_{\gamma,bary} f_* f_{esc} \qquad\qquad\quad m > m_{ref}(z) \\ & = N_{\gamma,bary} f_* f_{esc} (\frac{m}{m_{ref}(z)})^{\alpha} \quad m < m_{ref}(z) \end{array} \tag{31}$$

The power $\alpha = 2/3$ is to take into account the scaling of star formation found in low stellar mass galaxies (below $m_{stellar} = 3h \times 10^{10} h^{-1} M_{\odot}$) by Kauffmann et al (2003), we assume that it is the same for both starbursts and quiescent star formation as in the $z = 0$ sample low mass halos are not merging very often. We will call this scale m_{ref} in the following, our choices for it are discussed below. A similar mass dependence was introduced into $\zeta(m)$ by FMH05, but without the transition mass m_{ref}.

With a starburst, f_* will be larger (more gas will go into stars) for a time $\sim t_{burst} + t_*$ (that is, after the merger the number of baryons going into stars will increase, and these stars will add extra photons for their entire lifetime). The average $f_{*,burst}$ at this time is $f_{*,burst} t_* / (t_{burst} + t_*)$. Simulations of mergers at low redshifts provide some suggestions for f_* for a starburst, e.g. a range of 65% - 85% of the total gas (Mihos & Hernquist (1994; 1996)) or $\geq$80% of the cool gas (Springel, Di Matteo and Hernquist (2005)) going into stars (see also the studies of gas available at early times by Machacek, Bryan & Abel (2003)). Observationally, starburst star formation is fit by a decaying exponential with time scales as short at 20 Myrs in some examples but lasting up to hundreds of Myrs (e.g.Papovich, Dickinson & Ferguson (2001), Shapley et al (2001), Conselice (2006)) with similar time ranges used to analyze observed samples (Kauffmann et al (2003)).

We only consider Pop II stars, although it would be straightforward to generalize beyond this in our formalism. The transition redshift between creating Pop III stars and creating Pop II stars has been estimated to be

[9]Note that the photon production rate estimate in FO05 and in FMH05 has ζ time independent, and assumes that all mass going above $10^4 K$ is instantaneously converted into photons, which is another common approximation, e.g. Somerville & Livio (2003).

[10]We choose $f_{esc} = 0.05$ cf. Wyithe & Loeb (2003)), canonical choices vary by a factor of 10. Loeb et al use $N_{\gamma,bary} = 4300$ for a Scalo IMF of metallicity 1/20 of solar.

$z = 15$ (Yoshida, Bromm & Hernquist (2004), see Fang & Cen (2004) for more discussion of constraints on this transition); however a wide range of final redshifts where Pop III stars might be important for reionization have been suggested (between $z = 10$ and $z = 20$ e.g. Wyithe & Padmanabhan (2006), Wyithe & Cen (2006)). (There are even searches for evidence of Pop III stars at redshifts down to $z \sim 6$ (Scannapieco et al (2006)).) As a result we do not consider redshifts before $z \sim 12$ (which are active, for our choices of time scales, from mergers at $z \sim 15$).

There are expected differences at high redshift, for example the higher densities $\sim (1+z)^3$ lead to much shorter cooling times, as well as lower metallicities, thus these guesses are just that, however they are a starting point for estimating the size of time dependence of ζ.

3.2 Black Hole Accretion

We now turn to photon production due to black hole accretion of mass Δm. We take (again assuming a constant photon production rate and using the notation of Salvaterra, Ferrara & Haardt (2005)),

$$\frac{dN_{\gamma,bh}}{dt} = \Delta m c^2 \frac{f_{UV}}{\langle h\nu \rangle} \frac{\epsilon}{t_{acc}} \tag{32}$$

which leads to (using the time dependent version of eqn. 28)

$$\zeta_t(m_i, m_0, t_i, m, t) = 6.9 \times 10^7 \frac{\Delta m}{mX} \frac{\Omega_m}{\Omega_b} \frac{f_{UV}}{\frac{\langle h\nu \rangle}{13.6eV}} \frac{\epsilon}{t_{acc}} \tag{33}$$

The black hole photon production formula only applies to halos hosting a black hole (i.e. with mass above $m_{bh,min}(z)$) and includes the effects from UV photons only. The factor $\frac{f_{UV}}{\langle h\nu \rangle} = 0.1 - 0.2$ ryd^{-1} (e.g. Madau et al (2004)). We are assuming that f_{UV} takes into account any local absorption, i.e. it is the flux from the whole region due to the mass accretion. The efficiency is usually taken to be $\epsilon = 0.1$. The mass accreted Δm is often specified in terms of halo mass in the range $10^{-3} - 10^{-5} m$. Assuming the mass accretes at the Eddington rate

$$\dot{m_{bh}} = m_{bh}/t_S \ , \ \ t_S = 45 Myr (\epsilon/0.1)^{-1} \ , \tag{34}$$

and commonly used black hole mass to halo mass relations, $m_{bh} \sim 10^{-3} - 10^{-4} m$, this gives lifetimes t_{acc} from $0.01 - 10\ t_S$. We will take a relatively short accretion time, $0.1\ t_S$, as our fiducial time t_{acc} and $m_{bh} \sim 10^{-4} m$.[11]

[11] Many different concerns suggest a shorter t_{acc}. Relating the black hole mass instead to the halo velocity, $m_{bh} \sim 10^{-4}(1+z)^{3/2} m$ i.e. including redshift dependence (Bromley, Somerville & Fabian (2004),Wyithe & Padmanabhan (2006)), lowers t_{acc}. Accretion at super-Eddington rates (argued necessary to get super massive black holes by redshift 6 or 7, e.g. Haiman (2004)) also gives a shorter t_{acc}. In addition, shorter accretion times are also expected from some low redshift constraints based on the luminosity function (e.g. Wyithe & Padmanabhan (2006)).

For our purposes we consider all halos above some minimum mass $m_{bh,min}(z)$ to host black holes, and all halos below it not to host black holes, and ignore the scatter in this relation. We tried to estimate this minimum mass by using methods already found in the literature. We have two choices corresponding seed black holes at $z = 24$ in halos which are 3.5σ and 3σ fluctuations, following Madau et al's approach (2004), see the appendix for more discussion of this choice and constraints. The two cases used for minimum halo masses hosting black holes and $m(10^4K)$ are shown as a function of redshift in Fig. 1. Our fiducial model takes black hole hosts as 3.5σ fluctuations at $z = 24$, concordance cosmology, and the parameters in eq. 35. As mentioned earlier, we also explored some models with WMAP cosmological parameters: here a detailed application of the black hole halo constraints (some of which are described in the appendix) has yet to be done. However, in this case 3σ and 3.5σ halos at $z = 24$ have masses $11.3h^{-1}M_\odot$ and $600h^{-1}M_\odot$ respectively, which is difficult to reconcile (especially in the former case) with initial black hole masses of $\sim 100h^{-1}M_\odot$. We took one exploratory example: a black hole in 5 σ peaks at $z = 24$ (halos of mass $\sim 6 \times 10^5 h^{-1}M_\odot$). The motivation for the choice was that at least initially $m_{bh} \sim 10^{-3} - 10^{-4} m_{halo}$ and this limit is also shown in Fig. 1.

3.3 Recipe for Ionizing Photons

Combining the above, we have the following recipe for $\zeta_t(m_i, m_0, t_i, m, t)$ due to a m_i halo merging to mass m_0 at time t_i which later ends up in m at time $t < t_i + t_{ion}$: Besides the merger being within the t_{ion} of interest (starburst or accretion), the $\zeta_t(m_i, m_0, t_i, m, t)$ are also zero unless the masses also satisfy certain conditions. For the mass range cutoff for a major merger we will use 1:3 for starbursts (many ranges are used in the literature) and 1:10 for black hole accretion (e.g. Madau et al (2004)). For black holes $m_i > m_{bh,min}(z(t_i))$, for quiescent and starburst star formation $m_0 > \max(m(10^4K(t_i)), m_{0,min}(t_i))$.

Table 1: "Recipe" for $\zeta_t(m_i, m_0, t_i, m, t)$

cause	major merger	$m\zeta_t$	t_{ion}
quiescent	–	$\beta_{*,q}\frac{m^{1+\alpha}}{m_{ref}^{\alpha}}$	$t_* = 80$ Myr
starburst	$> 1:3$	$(\beta_{*,sb} - \beta_{*,q})\frac{m_0^{1+\alpha}}{m_{ref}^{\alpha}}$	$t_{burst} + t_* = 100$ Myr
black holes	$> 1:10$	$\beta_{bh} m_0$	$t_{acc} = 0.1\, t_S = 4.5$ Myr

Then β_*, β_{bh} encapsulate all the non-mass dependent factors:

$$\begin{aligned}
\beta_{*,q} &= f_* N_{\gamma,bary} \frac{f_{esc}}{t_*} \frac{1}{X} \\
&= \frac{.36}{\mathrm{Myr}} \frac{f_*}{0.1} \frac{N_{\gamma,bary}}{4400} \frac{f_{esc}}{0.05} \frac{80\mathrm{Myr}}{t_*} \\
\beta_{*,sb} &= \frac{1.5}{Myr} \frac{f_{*,burst}}{0.5} \frac{N_{\gamma,bary}}{4400} \frac{f_{esc}}{0.05} \frac{\frac{t_*}{t_{burst}+t_*}}{0.8} \\
\beta_{bh} &= 6.9 \times 10^7 \frac{\Delta m_0}{t_{acc} m_0} \epsilon \frac{\frac{f_{UV}}{\langle h\nu \rangle}}{\frac{1}{13.6eV}} \frac{\Omega_m}{\Omega_b X} \\
&= \frac{15.3}{Myr} \frac{f_{UV}/\langle h\nu \rangle}{0.1 ryd^{-1}} (\frac{m_{bh}/m}{10^{-4}}) (\frac{\epsilon}{0.1})
\end{aligned} \tag{35}$$

Our fiducial parameters are shown in the second line of each equation. Our fiducial $\alpha = 2/3$. The reference mass m_{ref} is taken to change with redshift,

$$m_{ref}(z) = 4.3 \times 10^{10} [\frac{\Omega_m(0)}{\Omega_m(z)} \frac{\Delta_{crit}(z)}{18\pi^2}]^{-1/2} (\frac{1+z}{10})^{-3/2} h^{-1} M_\odot \ , \tag{36}$$

(e.g. Wyithe & Loeb (2003)[12]). Some numerical studies have found a transition mass m_{ref} which doesn't change significantly with redshift (Keres et al (2005), the corresponding transition mass is also almost a factor of 10 smaller at $z = 0$).

For β_{bh} we estimate $\frac{\Delta m_0}{m_0 t_{acc}}$ assuming an Eddington rate and $t_{acc}/t_S \ll 1$ so that $\Delta m = m_{bh}(e^{t_{acc}/t_S} - 1) \sim m_{bh} t_{acc}/t_S$ and we take the black hole mass proportional to its host halo mass, $m_{bh} = 10^{-4} m_0$. The suggested relation of black hole mass to halo velocity mentioned earlier would give a larger ratio of black hole mass to halo mass and a bigger effect from black holes. In addition, super Eddington accretion will also shorten t_{acc} and increase β_{bh}. Note that changing $t_* + t_{burst}, t_{acc}$ also changes the range of integration for t_i in calculating ζ_t, not only the prefactors β_*, β_{bh}. For starburst star formation $f_{*,burst}$ gives an effective f_* of $f_{*,burst} t_* / (t_* + t_{burst})$.

With these assumptions, the $\zeta_t(m_i, m_0, t_i, m, t)$ in equation 5 are a set of constants for any given m_0 (or m for quiescent star formation). They are only nonzero when t_i, m_i, m_0 are in the right range, and for starbursts, black hole accretion or their combination. These constants were denoted as $\zeta_t^a(m_0)$ in section 2.4. All of these numbers rely on a huge number of estimates of unknowns, i.e. the contributions of starbursts, black hole accretion and their relative strengths. As mentioned earlier, ideally one could turn this around and use it to estimate the contributions from starbursts and quasars, but many uncertainties are involved. Here we are interested in the sporadic and time dependent nature of the mergers changing photon production rates.

Using these definitions, $\zeta_{t,a}(m)$ (equation 5) is shown in Fig. 2 for two black hole assumptions for a series of different times. The black hole and star formation contributions are shown separately as well. The quiescent

[12]They interpret the $m^{2/3}$ behavior as due to a potential well effect. We have taken their default parameter values for $v_* = 176$ km s^{-1} and $\Delta_{crit} = 18\pi^2 + 82x - 39x^2$, $x = \Omega_m(z) - 1$, $\Omega_m(z) = \Omega_m(0)(1+z)^3/[\Omega_m(0)(1+z)^3 + \Omega_\Lambda]$. At $z \geq 9$, $\Delta_{crit}/18\pi^2 \sim \Omega_m(z) \sim 1$.

contributions to $\zeta_{t,a}$ roughly scale with the dotted line in each case, but do not change with redshift. The ratio of merger-induced photon contributions to total photon contributions for our fiducial model and for the same redshifts is shown in Fig. 3. The source mergers have a similar photon production rate to the quiescent rate, increasing with increasing mass and redshift. There is also a sharp increase in the merger contribution relative to the quiescent contribution once the masses are large enough to host black holes. Although the black holes have a very large contribution per halo for high mass halos, the sharp decline in numbers of halos as mass increases somewhat limits their effects.

4 Consequences for bubbles

The framework and prescriptions of the previous two sections can now be combined to predict the resulting properties of the ionized bubbles. In practice there are two steps: $\zeta_t(m_i, m_0, t_i, m, t)$ is used to find the required overdensities for given bubble masses M, i.e. δ_M. The barriers δ_M then determine the bubble size distributions and the time evolution of the ionization fraction.

Our fiducial model, shown unless otherwise stated, is for the 3.5σ seed black holes at z=24 as described earlier and in the appendix, with parameters given in eqn. 35. We also considered 3σ seed black holes at $z = 24$, $\alpha = 0$, m_{ref} constant, $f_* f_{esc} \rightarrow 4 f_* f_{esc}$, no stars, no black holes. As mentioned above, we also varied the cosmology in several ways. We considered $\Omega_b h^2 = 0.0225$ leaving all else fixed and cosmological tilt $n = 1.05$ leaving all else fixed. The latter model seemed to have very similar effects to the one increasing $f_* f_{esc}$. We took some combinations of the variations with each other as well. The two lower integration limits for m_0, ($m_{0.min} = 0.1m$ or $m_{0,min} = m(T = 10^4 K)$) gave very similar results when $\alpha = 2/3$. We considered minihalo and MHR recombination for all the models, and MIPS recombination for the fiducial model and 5 representative variations. One other quantity we must fix is an initial condition; this is discussed below.

4.1 Barriers

To find the required δ_M given a bubble mass M we use the generalization of equation 3, equation 11:

$$\int^t dt' [(\zeta f)_{t'} - A_u (1 + \delta_{R,M}(t')) \frac{M_{ion}}{M} C(R_{ion}(t'))] = 1 \, . \tag{37}$$

Because time dependence is built in, we either need to integrate all the way back to the time of the very first ionizing photon production or include some initial condition of global ionization fraction. We choose to fix an initial condition at $z = 12$. At $z = 12$ halos are only active from mergers since

$z \sim 15$ with our choices of relaxation times. As discussed earlier $z = 15$ is the earliest redshift Pop II star dominance (and thus our assumptions) might be expected to hold.

The distribution corresponding to the initial photons is taken to be a time independent $\zeta(m)$ similar to the form given by FMH04 & FMH05, so either ζ_{FMH} is constant or

$$\zeta_{FMH} \propto \begin{cases} (\frac{m}{m_{ref}})^{2/3} & m < m_{ref} \\ const & m > m_{ref} \end{cases} \tag{38}$$

in accordance with the mass dependence of our ζ_t ($\alpha = 0, 2/3$). Then ζ_{FMH} is normalized by setting the global ionization fraction

$$\lim_{M\to\infty,\delta_M\to 0} \int dm \zeta_{FMH}(m) P_1(m, t_{bc}|M, \delta_M) = \bar{x}_{i,bc} \; . \tag{39}$$

At a later time, the ions present in a region of mass M with overdensity δ_M are a combination of the ions produced in that region at the initial time plus those produced since, minus recombinations:

$$\begin{array}{l} \int dm \zeta_{FMH}(m, t_{bc}) P_1(m, t_{bc}|M, \delta_M) \\ \quad + \int_{t_{bc}}^{t} dt' [(\zeta f)_{t'} - A_u(1 + \delta_{R,M}(t')) \frac{M_{ion}}{M} C(R_{ion}(t'))] = 1 \; . \end{array} \tag{40}$$

For our fiducial model, we start with an ionization fraction $\bar{x}_i(z = 12)$ of almost zero (10^{-3}). This should isolate the evolution of bubble properties due to the change in photon production since the initial time. We also experimented with some non-negligible initial photon distributions at $z = 12$ ($\bar{x}_i = 10^{-2}, 10^{-1}, 0.5, 0.14$) and an initial condition of $\bar{x}_i = 10^{-3}$ at $z = 16$ when halos are active from mergers since $z = 23$. This last corresponded to $\bar{x}_i = 0.16$ at $z = 12$. In practice at $z = 16$ Pop II stars are much less likely and our assumptions about photon production rates suspect, as a result this model was not our fiducial model, but is useful for studying effects of initial conditions.

To find $R_{ion}(t)$ the integral is divided into 700 steps from the initial time to the redshift of interest. At each time, the instantaneous change in ionized mass fraction $(\zeta f)_t dt$ is added to the mass fraction already present (the integral up to that time) to find M_{ion}/M, the ionized mass fraction. In the case where more photons were produced than hydrogen atoms in the region, we took $M_{ion}/M \equiv 1$ (allowing it greater than one had a neglible effect). We took $R_{ion} = [\frac{M_{ion}}{\frac{4\pi}{3}\bar{\rho}(1+\delta_{R,M}(t))}]^{1/3}$, however replacing $\frac{3M_{ion}}{4\pi} \to M_{ion}$ or even $\frac{3M}{4\pi}$ had very small effects on the resulting barriers we found; the biggest effect is due to the overall coefficient for recombinations, $\frac{M_{ion}}{M}$. Larger numbers of steps gave indistinguishable results.

We show in Fig. 4 examples of the resulting barriers δ_M at z=7, 8, 9, 10, 11 and 11.9 for our fiducial model and the three recombination prescriptions.

At large radius, $C_{MHR}(R)$ tends to approach a constant, C_{MIPS} is constant, and $C_{mh}(R)$ increases exponentially. Thus the barriers for minihalo recombination are cut off at large radius. MIPS and MHR recombinations allow bubbles to get very large, if there is sufficient photon production, to the point where consistency questions involving e.g. travel times within the corresponding bubbles arise. For plots of many of the models we thus choose to only include the cases with radii $< 100h^{-1}Mpc$, models with much larger radii do appear but are difficult to interpret.

Our time dependent approach produces results which interpolate between the two limits used in earlier works (e.g. FZH04,FO05,FMH05): they included implicit recombinations at early times, and imposed equilibrium between instantaneous photon production and recombination rates at late times. These two limits, in terms of δ_M, give the following: the early time approximation produces a barrier similar to ours for small M, approaching a constant (horizontal line as function of M) for large M. The late time (larger M) limit gives a barrier δ_M that is very close to a vertical line (see for example FO05, Fig.7), combining the early and late time limits gives the barrier we found which rises at both low and high M. Physically, for small bubbles, the photon mean free path exceeds the bubble radius, thus photons escape freely and recombinations do not play an important role; this is expected to happen at early times. As bubbles grow in size, the barriers for ionized regions decrease as a function of bubble radii, since more and more mass (and therefore ionizing photons) can be included in the region. At late times, bubble radii grow to exceed the photon mean free paths and recombinations limit the growth of bubbles. Of the three assumed IGM gas density distributions, the minihalo and MIPS models put more stringent constraints on the bubble growth than the MHR model. The stronger effects of minihalo recombination compared to MHR recombination were also observed in the models equating instantaneous recombination and photon production (FMH05 and FO05).

4.2 Bubble Size Distribution

The barriers found as a function of bubble radii translate directly into a bubble "mass function" $n_b(M, \delta_M)$ which gives the number density of bubbles with masses between M and $M + dM$. Descriptions of how to derive the resulting bubble mass function $n_b(M, \delta_M)$ for linear barriers can be found e.g. in Sheth & Tormen ((1998)) and McQuinn et al ((2005a)). As the barriers here are non-linear in $\sigma^2(M)$, we find $n_b(M, \delta_M)$ by simulating 4000 random walks directly for each (M, δ_M) combination. For linear barriers, 4000 steps reproduced the ionization fractions to a 5-10% percent once $\bar{x}_i > 0.01$.

The quantity $n_b(M, \delta_M)dM = Mn_b(M, \delta_M)d\ln M$ counts the number of bubbles with log mass $\ln M$. One might want this quantity if one knows

one has a collection of bubbles and wants to know the size distributions of these bubbles. However, for many questions it is of interest to know the fraction of mass in the universe in ionized bubbles with $\ln M$ in the range $\ln M$ to $\ln M + d\ln M$, i.e. $\frac{M^2}{\bar{\rho}} n_b(M, \delta_M) d\ln M$. This peaks at a larger mass than the former quantity due to the added factor of M. The peak of this distribution corresponds to a mass M_c with a characteristic radius $R_c = [3M_c/(4\pi\bar{\rho}(1+\delta_{R,M_c}(t)))]^{1/3}$. This radius (used also in earlier work, e.g. FMH05) denotes to the bubble size which contains the largest fraction of the ionized mass. The quantity $\frac{M^2}{\bar{\rho}} n_b(M, \delta_M) d\ln M$ is dimensionless and can also be thought of as probability distribution for $P(\ln M) d\ln M = P(\ln R) d\ln R$ (however it integrates to $\bar{x}_i$ rather than to one). This distribution and R_c are the quantities shown/derived in previous work, e.g. FMH05. The one big difference is that they divide by the overall ionization fraction $\bar{x}_i$. I.e. our plots give the fraction of the *total* mass which is in the ionized bubbles with the given $\ln M$. Our motivation for this is that the Monte Carlo calculations rely on counting paths crossing the barriers δ_M–with more fractional scatter in counts when there are fewer counts. By not including their factor $1/\bar{x}_i$ one can read off immediately which curves have the largest such sampling errors (i.e. the ones with the lowest heights).

In Fig. 5, we show R vs. $3\frac{M^2}{\bar{\rho}} n_b(M, \delta_M) = P(\ln R(M))$ for the sequence of different redshift barriers of Fig. 4 above. The trends shown here were seen in our other models as well. For all the models, the radii and ionized mass fraction grow with time. The late time shape of the distribution in $\ln R$ has a strong dependence upon the assumed form of recombinations. This is also shown in Fig. 7 below, lower left.

For minihalo recombinations the width of the probability distribution for R narrows as R increases and the universe ages. This schematically shows the progress of reionization: at early times bubbles are small and have a large range in sizes, depending more strongly on the local density and ionizing photon production where the bubbles live. As the global ionization fraction grows, or as the bubble volume filling factor increases, bubbles grow in size, slowed by recombinations. Finally bubbles saturate in radii and have similar sizes. In this scenario we expect to find small bubbles with a large scatter in size during early reionization, and large bubbles with similar sizes at late reionization. The narrowing of bubble width with increased ionization fraction was also seen in the studies of limiting cases in earlier work.

For MHR recombinations, the bubble distributions do not narrow at late times, instead recombinations are so weak that the bubble sizes tend to have runaway behavior, getting larger and spreading more as reionization proceeds. In the examples shown, MIPS recombinations are seen here to limit the growth of bubble regions, simply because MIPS recombinations are so much larger in number than MHR recombinations. However, in models where more photons are present (large $\bar{x}_i$) the radial distribution for MIPS

models moves to large R as is seen in the MHR case above for late times (large $\bar{x}_i$).

4.3 Ionization Fraction

The global ionization fraction is the fraction of mass inside bubbles at any given time; time histories are shown in Fig. 6 for the MHR, minihalo and MIPS recombination ansatze with the fiducial photon production model. Even with negligible photons present initially, the ionization fraction gets close to 1 by $z = 7$ for minihalo and MHR recombinations. For comparison, a model similar to FMH05 is also shown (given by equation 38). At early times the ionization fraction grows more slowly for this time independent ζ model as the mergers increase photon production as a function of mass more steeply than the $m^{2/3}$ slope. At late times recombinations become more important in the full models and slow reionization, hence, relative to them $\bar{x}_i$ for the FMH05 model increases more quickly. The cases for stars only and 3.5σ black holes only are shown as well. At late times the ionization fraction in the stars only model increases relative to the black holes only model, in part this is due to the rise in the black hole minimum host halo mass and the stronger decline in black hole merger photon production with redshift as seen in Fig. 2.

4.4 Scatter: model variations

There is scatter in the results both from model-to-model variations and from the merger-induced scatter within one model. The former represents uncertainties in the modeling, the latter scatter is expected even if the input parameters are perfectly known.

In order to see similarities and variations between models, we show four different comparisons in Fig. 7. The first model to model scatter we consider is that due to the unknown initial conditions for our formalism. The two top plots show the effects of the $z = 12$ initial conditions on the ionized mass fraction for different redshifts. The curves are for the fiducial $\bar{x}_i(z = 12) = 10^{-3}$ model and $\bar{x}_i(z = 12) = 10^{-2}, 10^{-1}$. At right we show the fiducial model and $\bar{x}_i(z = 12) = 0.5$. By $z = 10$ all the models with $\bar{x}_i$ at $z = 12 \leq 0.1$ predicted close to identical bubble radii distributions. The model with $\bar{x}_i = 0.5$ at $z = 12$ has the radii and ionization fraction changing much more slowly between $z = 12$ and $z = 9$, and then converging to the other cases. In addition, the $\bar{x}_i(z = 16) = 10^{-3}$ and $\bar{x}_i(z = 12) = 0.16$ models (sharing the same $\bar{x}_i$ at $z = 12$, not shown above) gave extremely similar radial distributions to each other at the redshifts above.

The bottom two plots consider a sampling of different models: different redshifts, photon production rates, recombinations, cosmologies, etc. At

lower left models with similar $\bar{x}_i$ but otherwise widely varying assumptions are shown. For low global ionization fraction the different models give distributions that are quite similar, irrespective of recombination method (and other properties such as redshift or photon production methods). For high global ionization fraction the distributions depend much more strongly on recombination methods and not only the global ionization fraction $\bar{x}_i$. The $\bar{x}_i \sim 0.95$ models with MHR recombination peak to larger R relative to the minihalo recombination models. The characteristic radius R_c for several hundreds of our model variants is shown at lower right, the general trend of larger radii corresponding to larger ionization fraction is clearly visible, with a spread that can be read off of the plot.

4.5 Scatter: merger induced for a fixed model

The scatter in the photon production rates for a given model due to mergers was described in §2.4. To propagate the scatter in photon production rates calculated from Eq. (27) to the scatter in bubble barriers, we replace

$$\int dt(\zeta f)_t \rightarrow \int (\zeta f)_t \pm \sqrt{\Delta(\int (\zeta f)_t dt)^2 + \sigma_{ic}^2} \tag{41}$$

in Eq. (40). We add the scatter of the initial condition (σ_{ic}^2, corresponding to the first term in equation 40) in quadrature to $\Delta(\int(\zeta f)_t dt)^2$. We take this initial condition scatter to also be Poisson in accord with our assumption (and that of FMH05) that the initial condition sources are Poisson distributed in the bubbles. The resulting barriers (overdensities) are those required for a region of mass M to be ionized if the sources within have the one-sigma fluctuation calculated above.

The corresponding barriers for the fiducial model are shown at $z = 10$ in Fig. 8, for all three recombination models. The central line indicates the average barriers δ_M, while the higher (lower) barrier $\delta_{M\pm}$ corresponds to the smaller(larger) photon production rate of one sigma fluctuations in $(\zeta f)_t$. At small bubble radii, the scatters around the mean values are large, while at the largest radii, the three barriers converge to the (recombination dependent) limiting bubble radius. There are two effects. Smaller bubbles presumably contain fewer halos, so the scatter of photon rates per source plays a relatively important role in determining the required overdensity for bubbles; conversely, the largest bubbles contain more halos and thus the effects of the scatter tend to average out within. In addition the barriers and thus radii for the scattered and not scattered cases converge when they hit the limiting value set by recombinations. At later times the distribution of ionized mass fraction as a function of R becomes more and more skewed to large radii, causing the characteristic radius to converge with this limiting radius. This trend was seen in all the cases where a limiting radius was found.

Producing fewer photons can lead to a scatter up or down in bubble radius: fewer photons means fewer ions all around, but the bubbles present are often required to be larger in order to enclose a sufficient number of sources. As in the case without scatter, for low R MHR, MIPS and minihalo recombinations are relatively weak and thus give similar results.

The corresponding radii distributions for these barriers are shown at top left and right and bottom left in Fig. 9. At bottom right the scatter is shown for the minihalo case for the model with $\bar{x}_i = 10^{-3}$ at $z = 16$, for the corresponding fiducial model with $\bar{x}_i = 0.16$ at $z = 12$ and for this fiducial model with the scatter doubled. The scatter for the model evolved from $z = 16$ converges to that starting at $z = 12$ by $z = 10$.

The full ionized mass fraction distribution is found by combining the scattered barriers and the mean one in a distribution, with some weighting. This weighting should correspond to outcome of the following procedure. In principle there is a sequence of barriers corresponding to adding and subtracting the fluctuations with a continuous coefficient rather than just the two cases above, with larger coefficients having smaller weights in the joint distribution. Each random walk used to find the ionized mass fraction then has a different barrier ("walk barrier") sampled from this distribution of barriers. At large scales all the walk barriers coincide, but at smaller scales fluctuations between different possible barriers come into play to give a range of walk barriers. The first crossings of each walk barrier are dependent both on the shapes of the barriers in the distribution and on the scales at which each barrier appears. A fluctuation from a higher barrier down to a lower barrier in a walk barrier at some mass M will produce first crossings not only of a path which was counted in the ionized mass fractions shown above, but also of any path which would have had first crossings earlier for this lower barrier but didn't for the higher barrier. If there was only one such transition between the barriers above and it was at a fixed M for all walk barriers, there would be a large spike at the mass scale of the transition, due to all these paths being included at the same M. (Likewise a drop would be expected for a sole transition from a low barrier to a high barrier in a walk barrier.) We do not expect these extreme cases to occur for many walk barriers however, and the transition masses M will change as well. We make a rough estimate of the resulting distribution as follows. Most of the time the walk barrier will sample the different barriers often enough that a "pileup" of paths that would have crossed earlier, causing such a spike, should be suppressed, similarly for the sharp signal associated with a single jump up to a higher barrier. In general, we expect each walk barrier to sample our 3 barriers frequently, and effects from different walk barriers (different samplings of the barrier distribution) to average out, so that the resulting ionized mass fraction distribution becomes close to a weighted average of the corresponding distributions for the 3 barriers shown above.

Some general trends were seen across many models and redshifts. The scatter effects for the families of models are summarized in Fig. 10 (as mentioned above MHR and MIPS cases with $R_c > 100h^{-1}$ Mpc are left out but models with $\alpha = 0$ are included). The final scatter (z=7) seems small in all other cases and the radii converge to a value independent of initial ionization fraction (but dependent upon each model's photon production rates). We call the peak (characteristic radius) of the distributions in R (such as above) for the scattered model R_{scat} and the peak for the fiducial model R_{ave} in these plots. The scatter decreases with increasing radius and decreasing redshift. This is shown in the upper and lower left plots: the upper left plot shows the effect of reduced scatter with increasing numbers of sources (R) included as mentioned earlier, at lower left is the redshift dependence. The ratio R_{scat}/R_{ave} also decreases as a function of increased ionization fraction $\bar{x}_i$, shown at upper right. As mentioned above, this is in part due to the ionization fraction profile becoming limited by recombinations as the ionization fraction grows, with the characteristic radius converging to the limiting radius. At lower right it is shown that the model-to-model scatter is often larger than the merger-induced scatter. The average curves for $3\frac{M^2}{\bar{\rho}} n_b(M, \delta_M)$, the fraction of total H in ionized H bubbles with a given $\ln R$ are shown for a series of models at $z = 9$ along with the representative scattered curves for one of them. Note that the mass ratios chosen to define a major merger will also affect the scatter, for example relaxing the major merger mass ratio leads to more mergers overall and thus smaller Poisson fluctuations.

4.6 Bubble Boundaries

One interesting question is how the ionization fraction decreases from 100% as one goes outside a fully ionized bubble at any given time (we thank Evan Scannapieco for suggesting this calculation and Steve Furlanetto for discussions about its interpretation). If the ionization fraction dropped from fully ionized to e.g. 90% ionized very slowly in space, or if bubbles were very close and connected by high density bridges, relaxing the constraint from fully ionized to 90% ionized would give a very different distribution of barriers and corresponding radii. To calculate the 90% ionized case we relax the complete ionization requirement for bubbles to

$$\begin{aligned} &\int dm \zeta_{FMH}(m, t_{bc}) P_1(m, t_{bc}|M, \delta_M) \\ &\quad + \int_{t_{bc}}^{t} dt' [(\zeta f)_{t'} - A_u(1 + \delta_{R,M}(t')) \tfrac{M_{ion}}{M} C(R_{ion}(t'))] = 0.9 \ . \end{aligned} \tag{42}$$

The bubble radii, for minihalo and MHR recombinations, are compared for 90% ionized and 100% ionized bubbles in Fig. 11. From Fig. 11 it is seen that these would-be bubbles tend to have very similar sizes compared to completely ionized bubbles. The main exception is when the global ionization

fraction is close to one for MHR recombination, perhaps indicating that a significant amount of bubble merging is occurring and/or that there are large regions near the bubbles (perhaps not in 100% ionized bubbles) with high average ionization fraction. For the above models and a sample of others, the fraction of mass 90% ionized or more is within 6% of the mass in regions which are fully ionized at $z = 7$, the difference increases to <15% at z = 11.

5 Conclusions

We have calculated contributions to $\zeta_{t,a}(m)$ including mergers, a time and mass dependent phenomena. We developed a time dependent description of the requirements for bubble formation (δ_M) that generalizes previous formulations. Using three recombination histories and several different parameterizations of the uncertain photon production, the requirements for bubble formation, characteristic radii and ionization fraction histories were then found.

Our results can be summarized as follows. The resulting solutions for δ_M from our formalism and calculations interpolate between the two limiting cases considered in previous work as expected. In comparison with these cases, the increased photon production due to mergers gives a faster rise in ionization fraction at early times, and then a slower one as recombinations become important. At early times the characteristic radii and distribution as a function of bubble radius for ionized mass depends most strongly on the global ionization fraction. At later times, the radial distribution for identical global ionization fractions depends strongly upon recombination prescriptions. The width of the distribution for the bubble radii narrows for minihalo recombinations at later times just as found in earlier work. For MHR and MIPS recombinations the distribution as a function of R widens once the ionization fraction is large. In addition, fixing global ionization fraction, the characteristic radius at late times tends to be larger for MHR and MIPS recombinations relative to minihalo recombinations. We also estimated the scatter between models (fairly large for different recombination prescriptions as described above, decreasing with time for similar models differing in initial conditions) and the scatter of radial distributions of the ionized mass within a given model. For the latter, recombinations (except when runaway behavior is present) limit the size of the largest bubbles independent of whether there is scatter present or not. As the global ionization fraction increases, the characteristic bubble size tends to this limiting size, resulting in characteristic bubble sizes with very small scatter as well. The model-to-model scatter tends to be larger than the merger induced scatter within a model.

We also explored variations using the WMAP cosmology parameters, with the seed black hole prescription mentioned earlier. Because the estimates of

the halo masses containing black holes are even more unconstrained for this case, and for simplicity, these models are not included in the plots above. Summarizing these cases, using the WMAP cosmology parameters and the accompanying family of models reduces strongly the number of photons, mostly because high mass halos are much rarer at early times. The WMAP models of radii vs. ionization fraction overlapped with those seen in Fig. 7–i.e. there was no additional spread introduced. The results for recombination dependence and ionization fraction followed the trends noted above. The WMAP cosmology with 5σ seed black holes gave larger scatter simply because there were fewer sources and hence the Poisson fluctuations were larger.

We also explored how the ionization fraction changed as the bubbles were required to not be fully ionized, but only 90% ionized. These mostly ionized bubbles had about the same amount of mass in them as the fully ionized bubbles, indicating that slightly relaxing the constraint of full ionization doesn't change the mass fraction contained in the relevant bubbles drastically.

The formalism and tools developed here and results found can be extended in future work. Many other parameter choices also fall well within the range of reasonable guesses due to the large uncertainties at early times, explorations of these would be very interesting. Pop III stars can be included in the same framework as well. The observational consequences of the trends we have identified in our models so far are also a clear next step. This can be done using analytic methods based on the distributions we have found. Another route would be to implement the ζ_t merger prescriptions into numerical simulations of histories or semi-analytic simulations such as those of Zahn et al (2006), and calculate the observational consequences this way.

Our methods to include mergers might also be useful to include in other descriptions of reionization, e.g. those which include the effects of clustering of galaxies such as is done by Babich & Loeb (2005).

We both thank the Aspen Center for Physics and the January winter meeting organizers for the opportunity to present this work when it was near completion. We are grateful to many people for helpful suggestions, pointers to literature and explanations, including A. Barth, M. Boylan-Kolchin, D.Eisenstein, J. Greene, J. Hennawi, G. Howes, I. Iliev, D. Keres, M. Kuhlen, C.P. Ma, A. Meiksin, C. McKee, M. Morales, P. Norberg, E. Quataert, B. Robertson, E. Scannapieco, R. Sheth, F. van den Bosch, A. Wetzel and O. Zahn. We want to thank S. Furlanetto in particular for numerous explanations and discussions and both him and E. Scannapieco for comments on the draft. We are very grateful to the anonymous referee for many suggestions and corrections that clarified the work discussed in this paper. Last but not least, JDC thanks M. White for more discussions about this topic than he ever wanted to have. JDC was supported in part by NSF-AST-0205935 and T.C. Chang was supported in part by NSF as well.

Appendices

Extended Press-Schechter definitions

Two probabilities appear in our formalism in the text. The probability that a halo of mass m at time t contains a halo of mass m_0 at time t_i is:

$$\begin{aligned} &P_1(m_0, t_i|m, t)dm_0 \\ &= \sqrt{\tfrac{1}{2\pi}}|\tfrac{d\sigma^2(m_0)}{dm_0}|\tfrac{\delta_c(t_i)-\delta_c(t)}{[\sigma^2(m_0)-\sigma^2(m)]^{3/2}}\exp\{-\tfrac{(\delta_c(t_i)-\delta_c(t))^2}{2(\sigma^2(m_0)-\sigma^2(m))}\}dm_0 \end{aligned} \tag{43}$$

The overdensity for collapse at time t_i is taken to be time dependent, $\delta_c(t_i) = 1.68/D(z_i)$ where $D(z_i)$ is the growth factor, and $\sigma_i^2 = \sigma(m_i)^2$ and $\sigma^2 = \sigma(m_0)^2$, the variance of the linear power spectrum smoothed over a region of mass m (at z=0).

The other quantity is the time derivative of the above, the fraction of halos that have mass m_0 that have jumped at time t_i from mass m_i:

$$\dot{P}_1(m_i \to m_0; t_i)\frac{m_0}{m_i}dm_i dt_i = \frac{1}{\sqrt{2\pi}}\frac{1}{(\sigma_i^2-\sigma^2)^{3/2}}[-\frac{d\delta_c(t_i)}{dt_i}]|\frac{d\sigma_i^2}{dm_i}|\frac{m_0}{m_i}dm_i dt_i \ . \tag{44}$$

The factor of m_0/m_i is added to convert from the number of points originating from m_i halos to the number of points in m_0 halos containing these earlier m_i halos.

To write the merger fraction, Eq.4, consider the following. The number of merged halos is the fraction of recently merged halos of mass m_0 at t_i times the number (density) $n(m_0, t_i)$ of m_0, t_i halos. Multiplying by their survival probability $P_2(m, t|m_0, t_i)$ of surviving to m, t gives the number (density) of m halos at time t which had a merger to mass $m_0 < m$ at this earlier time. Dividing the number of recently merged halos by the total number (density), $n(m, t)$ gives the recently merged fraction. We then multiply the fraction of halos which has a recent merger by the fraction of the total number of m, t halos found in a bubble of mass M, δ_M, i.e. by $n_h(m, t|M, \delta_M) = \frac{\bar{\rho}}{m}P_1(m, t|M, \delta_M)$ to give a number density. The product of these probabilities is then

$$\dot{P}_1(m_i \to m_0; t_i)\frac{m_0}{m_i}n(m_0, t_i)P_2(m, t|m_0, t_i)\frac{1}{n(m, t)}\frac{\bar{\rho}}{m}P_1(m, t|M, \delta_M) \tag{45}$$

which equals Eq. 4 because

$$P_1(m_0, t_i|m, t)n(m, t)\frac{m}{\bar{\rho}}dm_0 dm = P_2(m, t|m_0, t_i)n(m_0, t_i)\frac{m_0}{\bar{\rho}}dm_0 dm \tag{46}$$

(also this can be used to get an explicit expression for P_2). These probabilities are being multiplied together assuming that they are independent. There is the expectation that overdense regions should have larger merger rates (e.g.

Scannapieco & Thacker (2003), Furlanetto & Kamionkowski (2005)), however the overdensities here are in fact quite small (the bubble overdensities δ_M tend to be between 0 and 4 with corresponding physical overdensities $\delta_M D(z)$), so that this effect is expected to be small.

Minimum black hole masses

We describe here how we chose our minimum host halo masses for harboring black holes. For $m_{bh,min}(z)$ many suggestions of high redshift black hole histories are available, see for example the review by Haiman & Quataert (2004) and references therein. We take our black holes to be descendants of the very first stars, expected to be extremely massive due to the difficulty of fragmentation (see for example Bromm, Coppi & Larson (1999; 2002), Nakamura & Umemura (1999; 2001), Abel, Bryan & Norman (2000; 2002), Schneider et al (2002)). At the end of the lifetimes of these stars, very massive black holes are expected to form, e.g. Madau & Rees (2001), however the initial mass distribution of the stars and their resulting black holes are unknown (many different examples are considered in e.g. Alvarez, Bromm & Shapiro (2006), O'Shea et al (2005), Scannapieco et al (2006), and Madau et al (2004)).

We follow Madau et al (2004) and consider two cases, putting very massive black holes in all $> 3\sigma$ or $> 3.5\sigma$ fluctuations at redshift $z = 24$, corresponding to masses $m_{3\sigma}, m_{3.5\sigma}(m > 1.4 \times 10^5 h^{-1} M_\odot, m > 1.4 \times 10^6 h^{-1} M_\odot)$ which then grow primarily through mergers. We find the minimum mass for black holes at our (later) time of interest by requiring at least 90% of the halos with mass $m_{bh,min}(z)$ to have at least one halo of mass $m_{bh,min}(z = 24)$ in it, using extended Press-Schechter. (In practice it appears that at least 4 or 5 mergers occur for these high σ peaks by $z \sim 15$, we thus require at least the corresponding number of paths originally at mass m_1 to be present in each final mass halo of mass m at time t in order for that mass to host a black hole. We assume the black holes merge when their halos do, e.g. Mayer et al (2006), there is still discussion on this issue, see e.g. Madau et al (2004) for further discussion including considerations of black hole ejection.) A second option for estimating halo masses which can contain seed black holes is using the requirement of low angular momentum disks which can collapse, the two reference models for minimum black hole mass used by Koushiappas, Bullock & Dekel (2004) at $z = 9, 12, 15$ are approximately the same as those we find extrapolating the minimum mass halos of Madau et al (2004) for 3σ and 3.5σ host halos at $z = 24$. (For some reason Madau et al (2004) get a much lower merger rate than we do, ours is more in accord with the calculations of Koushiappas et al (2004).) As we are interested in some reasonable black hole mass estimates, the similarity between these two calculations suggests these are useful reference masses to consider. This is certainly not the only

way to estimate the black hole host masses, other options include tracing the luminosity function back in time e.g. Wyithe & Loeb (2002).

Black hole radiation in principle constrains black hole masses and numbers. However, compounding the the black hole/host halo mass relation uncertainties and accrection mode/speed uncertainties mentioned earlier are even more uncertainties tied to black hole radiation estimates. Harder X-ray photons may induce additional ionizations (some estimates have X-rays dominate the luminosity, e.g. Madau et al (2004)) in regions with low ionization fractions, in addition, efficiencies might be higher (Haiman & Quataert (2004)). The strongest direct constraints on early black holes is that they don't produce photons that exceed the unresolved soft X-ray background (Dijkstra, Haiman & Loeb (2004), Salvaterra, Ferrara & Haardt (2005)). This translates into a constraint on the ratio Φ of power law to multicolor disk luminosities; although we use Madau et al's (2004) original model of including black holes we take $\Phi < 1$ to avoid the constraints their models could not satisfy ($\Phi \sim 0.1$ is common today). Other black hole halo mass constraints requiring more evolutionary assumptions over longer periods of time include predicting correctly black hole to halo mass ratios today (e.g. Ferrarese & Merritt (2000)), the number of intermediate mass black holes today (Yu & Tremaine (2002)) and the observed quasar activity observed up to $z \sim 6$. In addition, one expects starbursts and black hole growth can be related using the relation between central black hole mass and bulge velocity dispersion [13], models proposed to do this explicitly include those by Cattaneo et al (2005) and Enoki et al (2003).

Other scatter assumptions

Other assumptions are possible for

$$\langle n(m,t|M,\delta_M)n(m',t'|M,\delta_M)\rangle \ . \tag{47}$$

and

$$\langle n^a(m_0|m,t)n^b(m_0|m,t)\rangle \ . \tag{48}$$

besides those used in the main body of this paper. We list two more possibilities for each.

For $\langle n(m,t|M,\delta_M)n(m',t'|M,\delta_M)\rangle$, one might expect that a large fluctuation at time t implies a large fluctuation at time $t' = t + \epsilon$, giving a correlation between different t, t'. In addition, halos of mass m at time t will have a different mass m' at time t', so the fluctuations will be related for $m \neq m'$ and $t \neq t'$.

[13] We thank Joe Hennawi for this suggestion.

One possibility is to give the scatter a decay time (or characteristic δ_{rel}) and a decay mass m_{rel},

$$\langle n(m,t|M,\delta_M)n(m',t'|M,\delta_M)\rangle = e^{-(\delta(t')-\delta(t))/\delta_{rel}}e^{-(\sigma^2(m)-\sigma^2(m'))/\sigma^2(m_{rel})}n(m,t) \tag{49}$$

Other possibilities are to have the decay depend on t rather than $\delta(t)$ and m rather than $\sigma^2(m)$.

Another possibility is to say that the relation between the mean values of $n(m,t|M,\delta_M)$ and $n(m',t'|M,\delta_M)$

$$\begin{array}{l} n(m,t|M,\delta_M)n(m',t'|M,\delta_M) = \\ n(m,t|M,\delta_M)\int dm'' P_1(m',t'|m'',t)\frac{m"}{m'}n(m",t|M,\delta_M) \\ m'<m, t'<t \end{array} \tag{50}$$

suggests a relation between the scatters for $m'<m, t'<t$ as follows:

$$\begin{array}{rl} \langle n(m,t|M,\delta_M)n(m',t'|M,\delta_M)\rangle & = \langle n(m,t|M,\delta_M)\int dm'' P_1(m',t'|m'',t)\frac{m"}{m'}n(m",t|m,t)\rangle \\ & = n(m,t|M,\delta_M)n(m',t'|M,\delta_M) \\ & +\frac{1}{V_M}\Theta(t-t')\int dm''\frac{m''}{m'}P_1(m',t'|m'',t)\delta(m-m'')n(m,t|M,\delta_M) \\ & = n(m,t|M,\delta_M)n(m',t'|M,\delta_M) \\ & +\frac{1}{V_M}\Theta(t-t')\ \frac{m}{m'}P_1(m',t'|m,t)n(m,t|M,\delta_M)\ ; \\ & m'<m, t'<t\ . \end{array} \tag{51}$$

and similarly when $(m,t)\leftrightarrow(m',t')$ when $m'>m, t'>t$. This is not required: the relation between the average values does not have to be followed by the scatter, it is an additional modeling assumption.

The equal mass and time limit, $m\to m', t\to t'$ can be taken in the above. Writing $\sigma^2(m')-\sigma^2(m)=x, \delta(t')-\delta(t)=y$ we have

$$P_1(x,y)=\frac{1}{\sqrt{2\pi}}\frac{y}{x^{3/2}}e^{-y^2/(2x)}\frac{dx}{dm}=-\frac{d}{dy}[\frac{1}{\sqrt{2\pi}}\frac{1}{x^{1/2}}e^{-y^2/(2x)}]\frac{dx}{dm}\ , \tag{52}$$

then $m\to m'$ is $x\to 0$ and $t\to t'$ is $y\to 0$. The two limits do not commute, thus another assumption is involved, we take $m\to m'$ first, roughly writing $\int dm = \int dm(\Theta(m-m')+\Theta(m'-m)+(\delta_D(m-m')-1))$ and then recognize the Dirac delta function as the $x\to 0$ limit of the quantity in square brackets. This also assumes taking this limit and taking the derivative commute. We then get the full two point function for these assumptions to be:

$$\begin{array}{l} \langle n(m,t|M,\delta_M)n(m',t'|M,\delta_M)\rangle = n(m,t|M,\delta_M)n(m',t'|M,\delta_M) \\ +\frac{1}{V_M}\Theta(t-t')\frac{m}{m'}P_1(m',t'|m,t)n(m,t|M,\delta_M) \\ +\frac{1}{V_M}\Theta(t'-t)\frac{m'}{m}P_1(m,t|m',t')n(m',t'|M,\delta_M) \\ -\frac{1}{V_M}\delta(m-m')\delta_D(\delta(t)-\delta(t'))n(m',t'|M,\delta_M) \end{array} \tag{53}$$

The derivative of $\delta_D(y)$ is evaluated by integrating by parts and changing variables to t,t'.

There is also a range of possibilities for the scatter in $\zeta_{t,a}(m)$ or $n^a(m_0|m,t)$. Again, we describe two.

One possibility is to take the same scatter as is used for $n(m,t|M,\delta_M)$ and use it for $P_1(m_0,t_i|m,t) = \frac{m_0}{\bar{\rho}} n(m_0,t_i|m,t)$ and then define the scatter for $\dot{P}_1(m_i \to m_0,t_i)$ as the limit. Naive attempts to take this limit give a divergence however.

One also might say that a halo of mass m_0 in a halo of mass m has either had or not had a recent merger, which suggests a binomial distribution, and that if the total number of halos of mass m_0 in m,t halos is N that this number is then pN, implying a scatter $Np - p^2N$ rather than the poisson N. Implementing this appears to require yet another assumption because the time integral of the rate appears, but it will decrease the scatter from Poisson ($\sim Np$).

None of these scatter prescriptions is required given current knowledge, thus in the main body of the text we used the simplest version. It is reasonable to expect that the trends of largest scatter for smallest radii will continue as large numbers of enclosed halos will tend to enclose the mean number of mergers.

References

[2000] Abel, T., Bryan, G., Norman, M.L., 2000, ApJ 540, 29

[2002] Abel, T., Bryan, G., Norman, M.L., 2002, Science, 295, 93

[2006] Alvarez, M.A., Bromm, V., Shapiro, P.R., 2006, ApJ 639, 621

[2005] Alvarez, M.A., Komatsu, E., Dore, O., Shapiro, P.R., 2005, astro-ph/0512010

[2001] A. Andreu, G. Gonzalez-Casado, E. Salvador-Sole, 2001, MNRAS 327, 939

[1972] Arons, J., Wingert, D.W., 1972, ApJ 177,1

[2005] Babich, D., Loeb, A., 2005, astro-ph/0509784

[2006] Bagla, J.S., Prasad, J., 2006, astro-ph/0601320

[2001] Becker, R.H., et al, 2001, AJ 122, 2850

[1991] Bond, J.R., Cole, S., Efstathiou, G., Kaiser, N., 1991, ApJ 379, 440

[2001] Barkana, R., Loeb, A., 2001, PhR 349, 125

[2004a] Barkana, R., Loeb, A., 2004, ApJ 609, 474

[2005] Barkana, R., Loeb, A., 2005, astro-ph/0510421

[2005] Benson, A.J., Kamionkowski, M., Hassani, S.H., 2005, MNRAS, 357, 847

[1991] Bower, R., J., 1991, MNRAS, 248, 332

[2004] Bromley, I.M., Somerville, R.S., Fabian, A.C., 2004, MNRAS, 450, 356

[1999] Bromm, V., Coppi, P.S., Larson, R.B., 1999, ApJ, 527, L5

[2002] Bromm, V., Coppi, P.S., Larson, R.B., 2002, ApJ, 564,23

[2002] Casas-Miranda, R., Mo, H.J., Sheth, R.K., & Boerner, G., 2002, MNRAS 333, 730

[2005] Cattaneo, A., Blaizot, J., Devriendt, J., Guiderdoni, B., 2005, MNRAS 364, 407

[2000] Cavaliere, A., Vittorini, V., 2000, ApJ, 543, 599

[2003] Ciardi, B., Stoehr, F., White, S.D.M., 2003, MNRAS, 343, 1101

[2006] Ciardi, B., Scannapieco, E., Stoehr, F., Ferrara, A., Iliev, I.T., Shapiro, P.R, 2006, MNRAS 366, 689

[2006] Conselice, C.J., 2006, ApJ 638, 686

[2006] Cooray, A., Barton, E., eds., 2005, "First Light and Reionization: Theoretical Study and Experimental Detection of the First Luminous Sources", New AR 50

[2006] Dave, R., 2006, NewAR 50, 24

[2004] Dijkstra, M., Haiman, Z., Loeb, A., 2004, ApJ 613, 646

[1997] Einsenstein, D, Hu, W., 1997, Apj 511, 5

[2003] Enoki, M., Nagashima, M., Gouda, N., 2003, Publications of the Astronomical Society of Japan, 55, 133

[2003] Fan, X., et al 2003, AJ, 125, 1649

[2006] Fan, X., Carilli, C.L., Keating, B., 2006, astro-ph/0602375, ARA&A to appear.

[2004] Fang, T., Cen, R., 2004, ApJL 616, 87.

[2000] Ferrarese, L., Merritt, D., 2000, ApJ 539, 9L

[2004] Furlanetto, S.R., Briggs, F. H., 2004, New Astronomy Review, 48, 1039

[2004] Furlanetto, S.R., Hernquist, L., Zaldariagga, 2004, MNRAS, 354, 695

[2004a] Furlanetto, S.R., Zaldariagga, M., Hernquist, L., 2004, ApJ 613, 1

[2004b] Furlanetto, S.R., Zaldariagga, M., Hernquist, L., 2004, ApJ 613, 16

[2006] Furlanetto, S.R., Zaldariagga, M., Hernquist, L., 2006, MNRAS, 365, 1012

[2005] Furlanetto, S.R., McQuinn, M., Hernquist, L., 2005, 2006, MNRAS 365, 15

[2005] Furlanetto, S.R., Oh, S.P., 2005, MNRAS 363, 103

[2005] Furlanetto, S.R., Kamionkowski, M., 2005, astro-ph/0507650

[2001] Jang-Condell,H., Hernquist, L., 2001, ApJ 548, 68

[2000] Gnedin,N.Y. 2000, ApJ 535, 530

[2004] Haiman, Z., 2004, ApJ, 613, 36

[2004] Haiman, Z., Quataert, E., 2004, in *Supermassive Black Holes in the Distant Universe*, Ed. A.J.Barger, Kluwer Academic Publisher, Dordrecht.

[2006] Heitmann, K., Lukic, Z., Habib, S., Ricker, P.M., 2006, astro-ph/0601233

[2005] Iliev, I.T., Scannapieco, E., Shapiro, P.R., 2005, ApJ 624, 491

[2005] Iliev, I.T., et al, 2005, MNRAS 361, 405

[2006] Mellema, G., Iliev, I.T., Pen, U.-L., Shapiro, P.R., 2006, astro-ph/0603518

[2000] Kauffmann, G., Haehnelt, M., 2000, MNRAS 311, 576

[2003] Kauffmann, G., et al., 2003, MNRAS 341, 54.

[2005] Keres, D., et al, 2005, MNRAS 363, 2

[1996] Kitayama, T. & Suto, Y., 1996, MNRAS 280, 638

[2005] Kohler, K, Gnedin, N.Y., Hamilton, A.J.S, 2005, astro-ph/0511627

[2004] Koushiappas, S.M., Bullock, J.S., Dekel, A., 2004, MNRAS, 354, 292

[1993] Lacey, C., Cole, S., 1993, MNRAS, 262, 627

[1994] Lacey, C., Cole, S., 1994, MNRAS, 271, 676

[2001] Loeb, A. & Barkana, R., 2001, ARA&A, 39, 19

[2005] Loeb, A., Barkana, R., Hernquist, L., 2005, ApJ 620, 553

[2006] Loeb, A., 2006, to be published by Springer, astro-ph/0603360

[2003] Machacek, M.M., Bryan, G.L., Abel, T., 2003, MNRAS, 338, 273

[2001] Madau, P., Rees, M.J., 2001, ApJ, 551, L27

[2004] Madau, P., Rees, M.J., Volonteri, M., Haardt, F., Oh, S.P., 2004, ApJ 604, 484

[2006] Mayer, L, et al, 2006, astro-ph/0602029

[2005a] McQuinn, M., Furlanetto, S.R., Hernquist, L., Zahn, O., Zaldarriaga, M., 2005, ApJ 630, 643

[2005b] McQuinn, M., Zahn, O., Zaldarriaga, M., Hernquist, L., Furlanetto, S., 2005, NewAR 50, 84

[1994] Mihos, J., Hernquist, L., 1994, ApJ, 425, 13

[1996] Mihos, J., Hernquist, L., 1996, ApJ, 464, 641

[2000] Miralda-Escude, J., Haehnelt, M., & Rees, M.J., 2000, ApJ 531, 1

[2002] Mo, H.J., White, S.D.M., 2002, MNRAS 336, 112

[1999] Nakamura, F., Umemura, M., 1999, ApJ, 515, 239

[2001] Nakamura, F., Umemura, M., 2001, ApJ, 548, 19

[2005] Naoz, S., Barkana, R., 2005, MNRAS 362, 1047

[2005] Oh, S.P., Furlanetto, S., 2005, ApJL 620, 9

[2005] O'Shea, B.W., Abel, T., Whalen, D., Norman, M.L., ApJ 628, L5

[2001] Papovich, C., Dickinson, M., Ferguson, H.C., 2001, ApJ, 559, 620

[1974] Press, W., Schechter, P., 1974, ApJ 187, 425

[1998] A. Raig, G. Gonzalez-Casado, E. Salvador-Sole, 1998, ApJ 508, L129

[2002] Razoumov, A.O., et al, 2002, ApJ 572, 695

[2003] Reed, D., et al, 2003, MNRAS 346, 565

[2005] Reed, D., et al, 2005, MNRAS 363, 393

[1998] E. Salvador-Sole, J.S. Solanes, A. Manrique, 1998, ApJ 499, 542

[2005] Salvaterra, R., Haardt, F., Ferrara, A., 2005,astro-ph/0507208, MNRAS in press

[2003] Scannapieco, E. & Thacker, R.J., 2003, ApJ 590L, 69

[2006] Scannapieco, E., et al, 2006, New AR 50, 89

[2002] Schneider, R., Ferrara, A., Natarajan, P., Omukai, K., 2002, ApJ 571, 20

[2005] Shapiro, P.R., et al, 2005, astro-ph/0512516

[2001] Shapley, A., E., 2001, ApJ, 562, 95

[1998] Sheth, R., 1998, MNRAS 300, 1057

[1999] Sheth, R., Lemson, G., 1999, 304, 767

[2002] Sheth, R., Tormen, G., 2002, MNRAS 329, 61

[2003] Sokasian, A., Abel, T., Hernquist, L., Springel, V., 2003, MNRAS, 344, 607

[2004] Sokasian, A., Yoshida,N., Abel, T., Hernquist, L, Springel, V., 2004, MNRAS 350, 47

[2003] Somerville, R.S. & Livio, M., 2003, ApJ 593, 611

[2006] Spergel, D. N. et al, 2006, to appear

[2005] Springel, V., Di Matteo, T., Hernquist, L., 2005, MNRAS 361, 776

[2005] Warren, M.S., Abazajian, K., Holz, D.E., Teodoro, L., 2005, astro-ph/0506395

[2004] White, R.L., et al, 2004, AJ 126, 1

[2005] White, R.L., et al, 2005, AJ 129, 2102

[2002] Wyithe, S.B., Loeb, A., 2002,ApJ, 581, 886

[2003] Wyithe, S.B., Loeb, A., 2003, ApJ, 586, 693

[2004] Wyithe, S.B., Loeb, A., 2004, Nature, 427, 815

[2006] Wyithe, S.B., Padmanabhan, T., 206, MNRAS 366, 1029

[2006] Wyithe, S.B., Cen, R., 2006, astro-ph/0602503

[2004] Yoshida, N., Bromm, V., Hernquist, L., 2004, ApJ 605, 579

[2002] Yu, Q, Tremaine, S., 2002, MNRAS, 335, 965

[2005] Zahn, O., et al, 2005, ApJ 630, 657

[2006] Zahn, O., et al, 2006, to appear. Presented at Aspen Winter Meeting Jan. 2006.

[2004] Zaldarriaga, M., Furlanetto, S., Hernquist, L., 2005, ApJ 608, 622

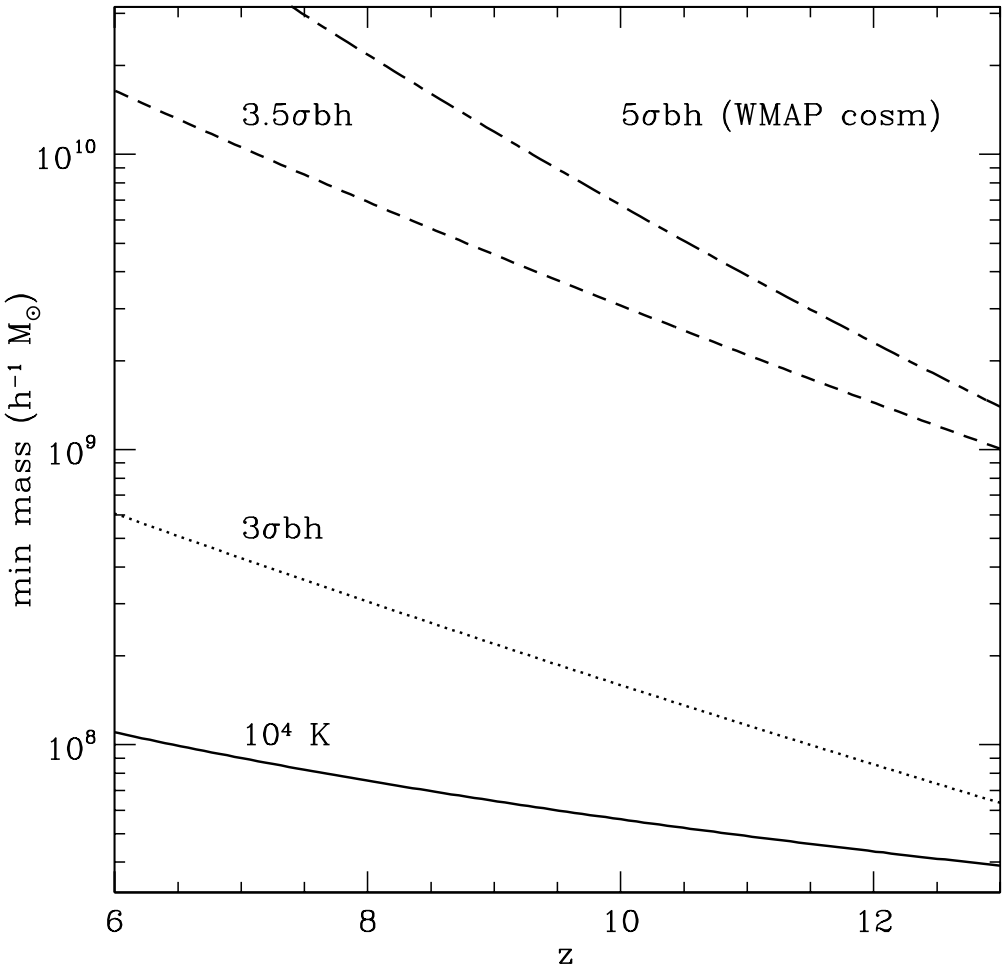

Figure 1: Minimum halo masses as a function of redshift. The lowest solid line is the mass of a $10^4 K$ halo. The top 3 lines show three models for the minimum mass for a halo to contain a black hole. They come from choosing black hole hosting halos at $z = 24$ which are respectively 3σ (dotted), 3.5σ (dashed), or 5σ (dot-dashed, uses WMAP cosmological parameters) peaks; see the appendix for details. Our fiducial model uses the 3.5σ seeds at $z = 24$.

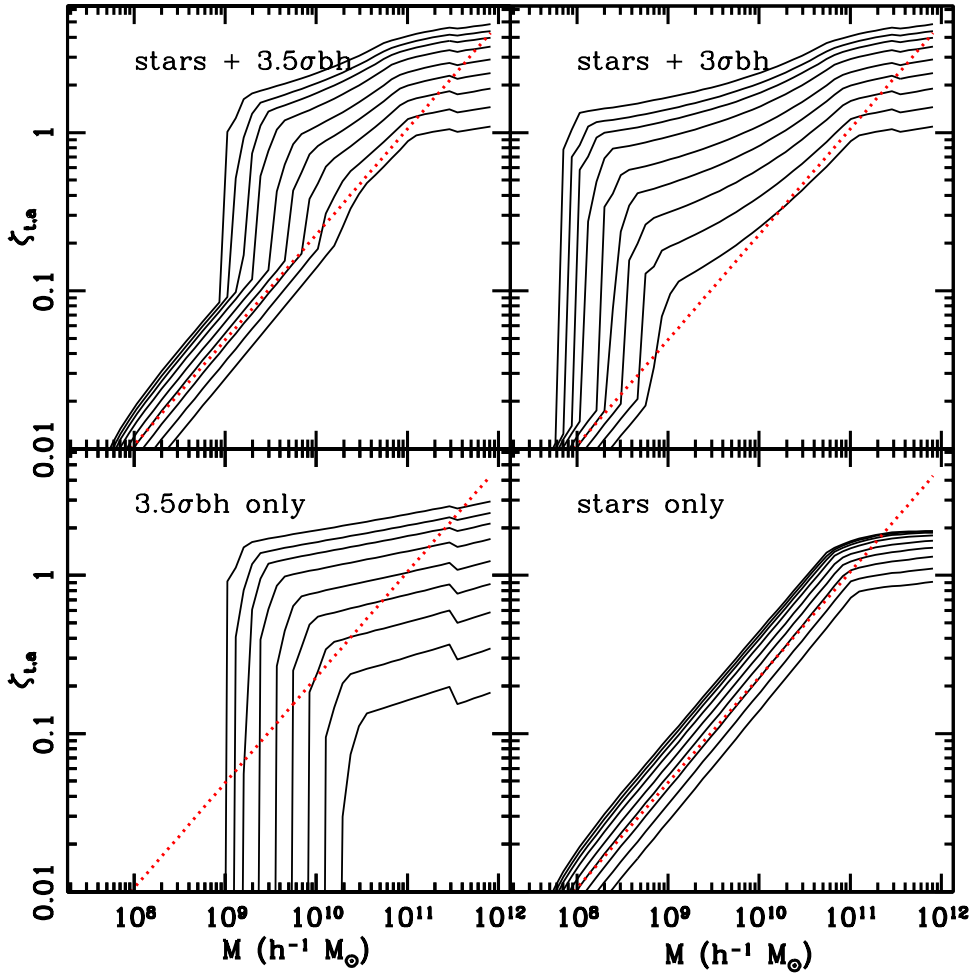

Figure 2: Redshift and mass dependence of $\zeta_{t,a}(m)$, lines are $z = 5.9, 7.1, 8.0, 9.0, 10.2, 11.2, 11.9, 12.6.13.4$, bottom to top (mergers are more common in the past, increasing photon production and thus $\zeta_{t,a}(m)$). Top left: stars and 3.5 σ black holes, top right: stars and 3σ black holes. Bottom left: 3.5 σ black holes only. Bottom right, stars only. The dotted line in each case is the slope that would arise from a time independent broken power law as described in eq. 38. Mergers steepen the slope slightly ($m^{2/3} \rightarrow\sim m^{0.7}$) at every redshift.

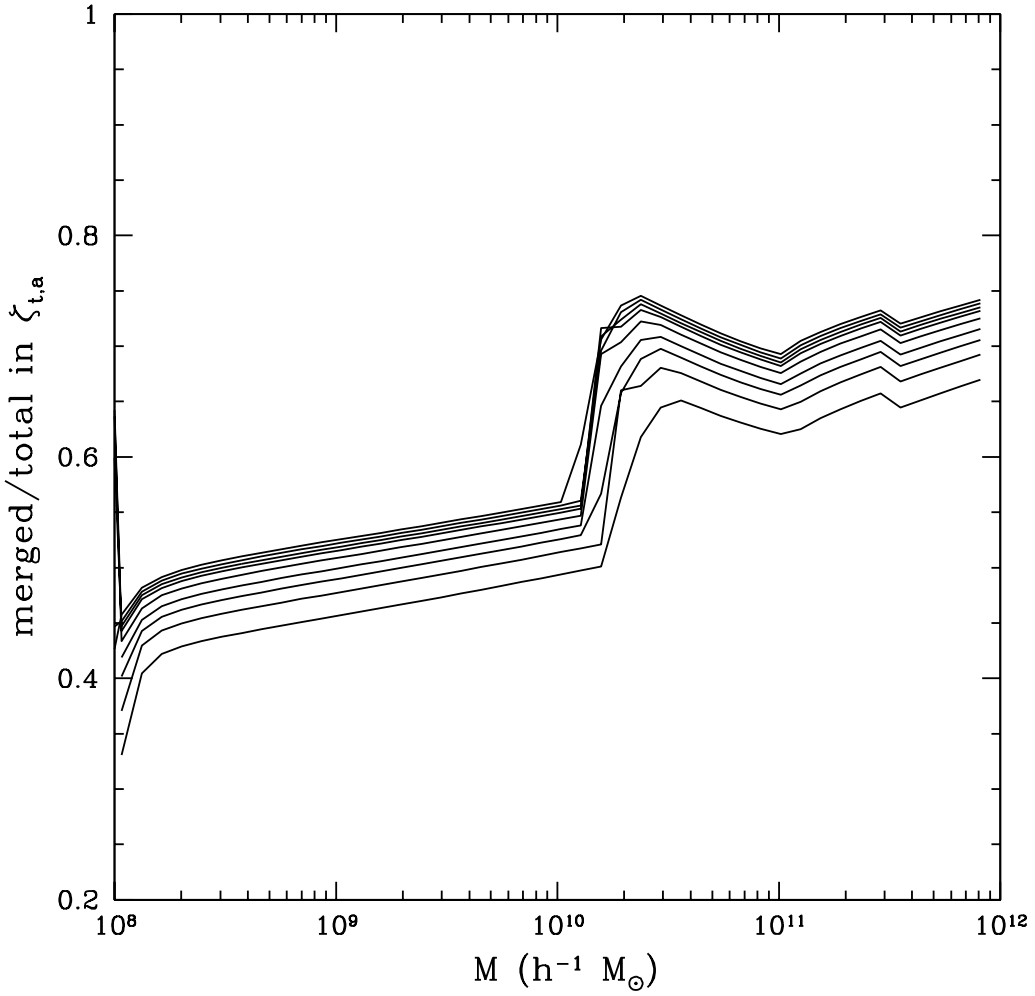

Figure 3: Ratio of photon production rates: merger-produced/(merger produced and quiescent) as a function of mass, for the same redshifts as Fig. 2, low to high redshift going bottom to top. The small wiggle immediately above the sharp rise is a numerical artifact.

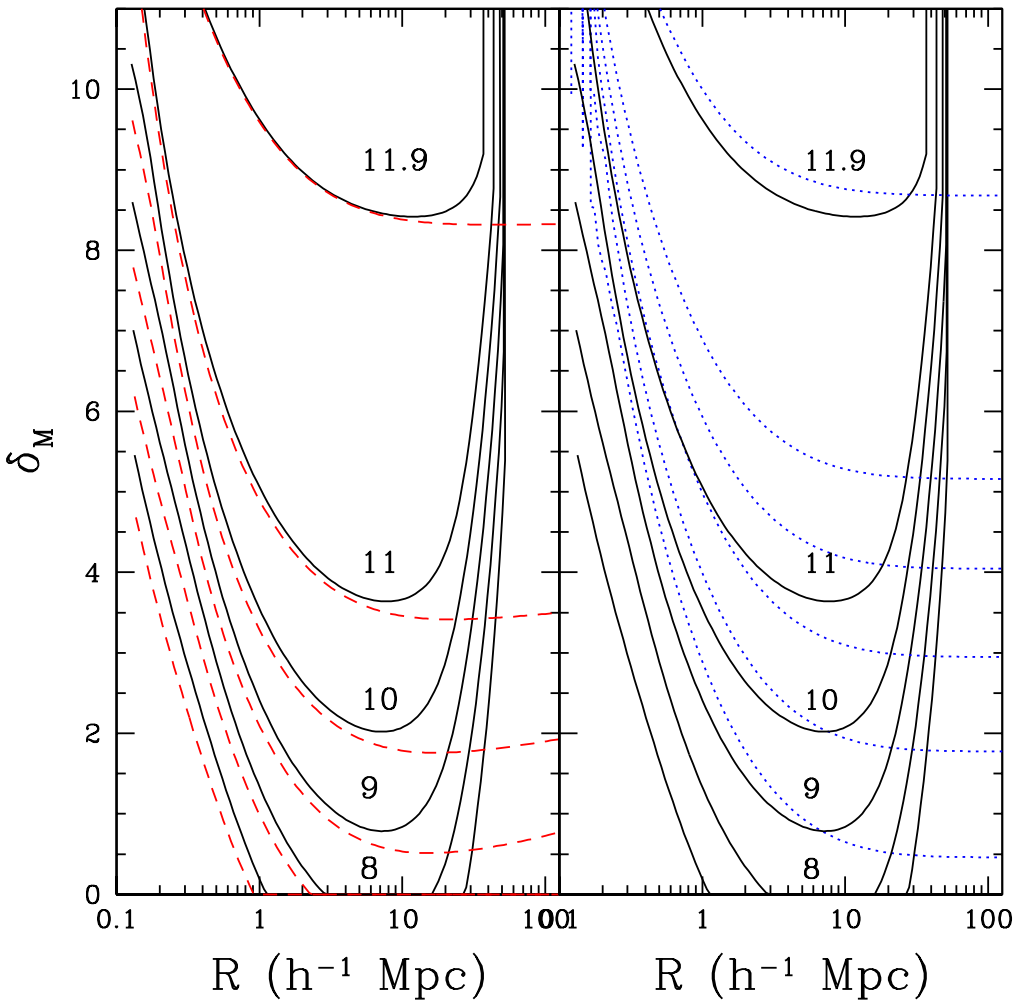

Figure 4: The barriers δ_M found at $z = 7, 8, 9, 10, 11, 11.9$ for our fidicial model. The solid lines (left and right) use minihalo recombination (eqn. 15 in text), the dashes (left) use MHR recombination (eqn. 13), and the dots (right) use MIPS recombination (eqn. 16). The redshifts for minihalo recombination are labelled, for MHR or MIPS they coincide at high z and then can be deduced by counting lines down.

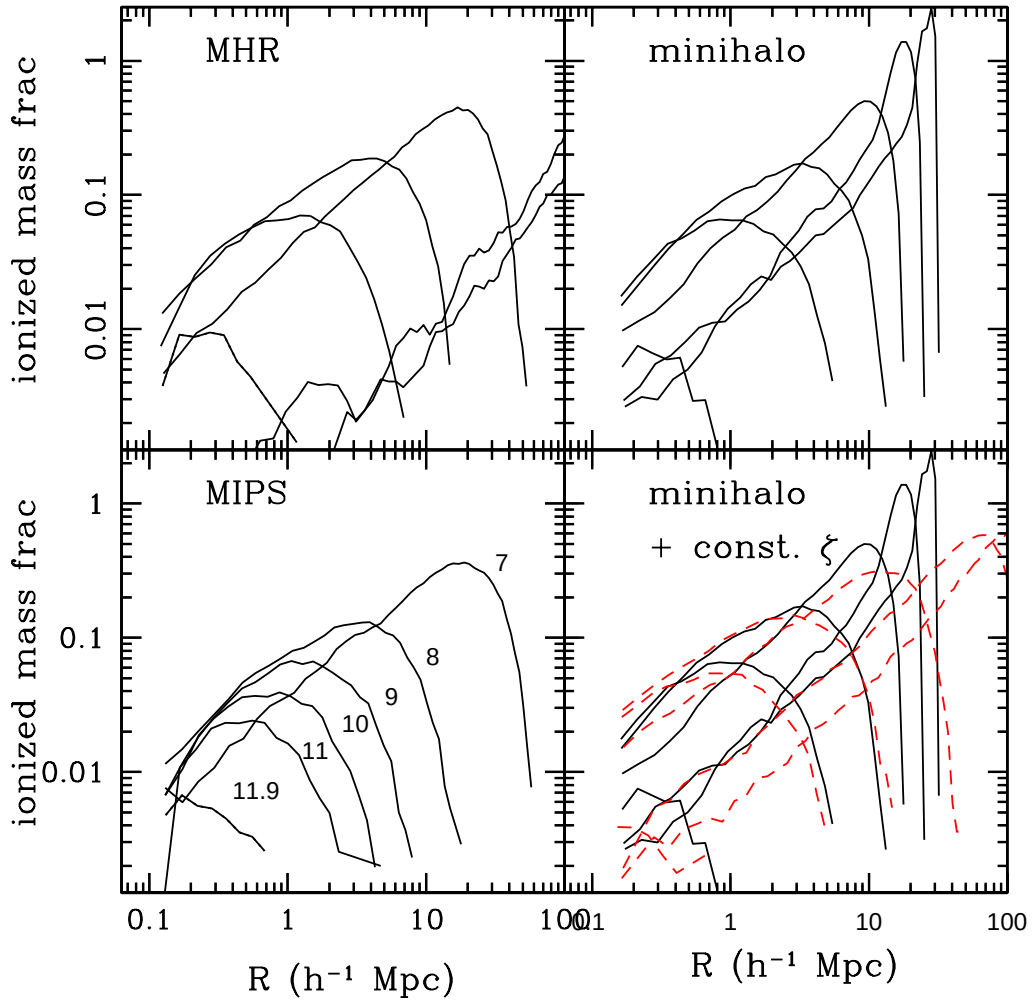

Figure 5: Top left and right and bottom left: ionized mass fraction ($3\frac{M^2}{\bar{\rho}} n_b(M, \delta_M)$, i.e. fraction of total mass), in bubbles of radius R for three recombination prescriptions. The lines are for different redshifts (11.9, 11, 10, 9, 8, 7), the smallest height curves are at the earliest time. The MHR recombinations are weakest and thus result in the largest bubbles, extending at late times to sizes where many other concerns arise as to interpretation of the model. At bottom right, the minihalo recombination model is shown again (solid line) along with a time independent zeta $\sim m^{2/3}$ model (eq. 38) having the same $\bar{x}_i$ at each redshift (dashed line). The time independent models have comparable central values of R for high redshifts and low ionization fractions, i.e. at early times when recombinations aren't very important. Generally their radial distributions are wider as their recombinations are only implicit.

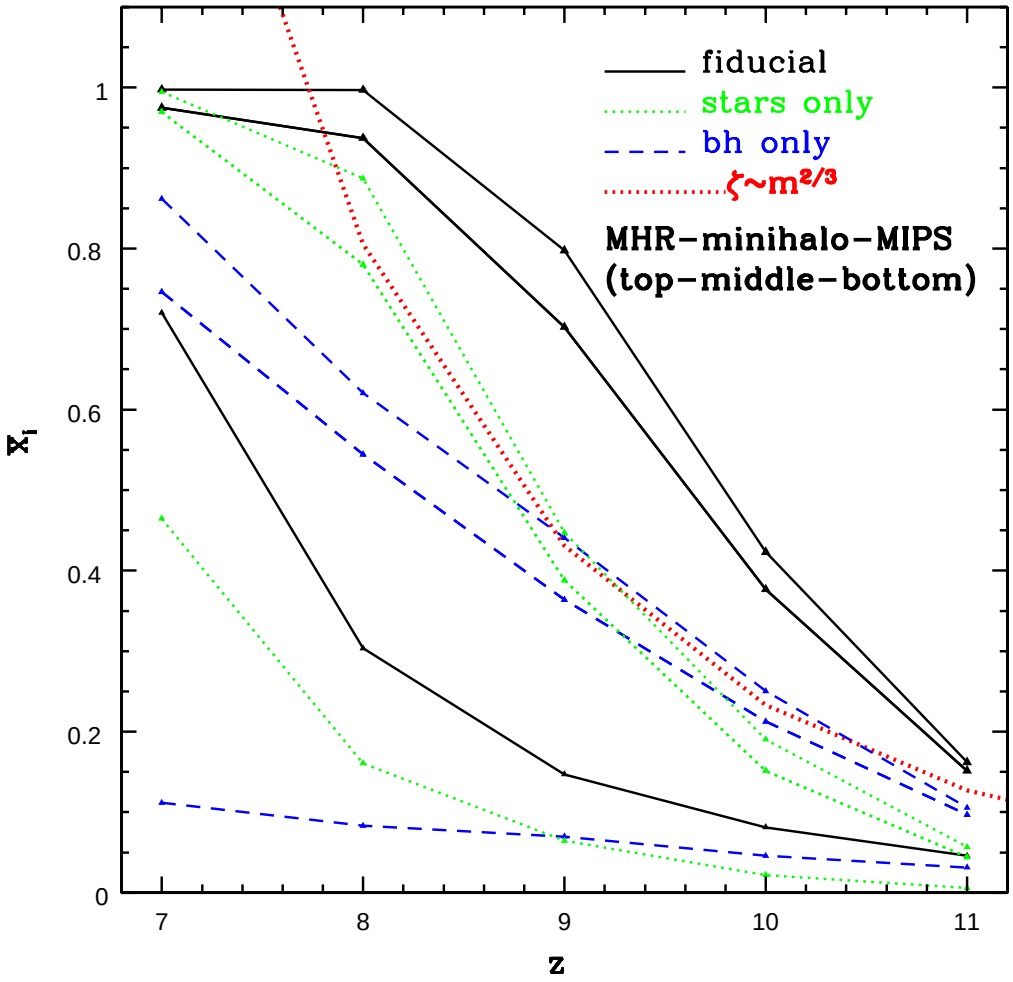

Figure 6: $\bar{x}_i$ as a function of redshift starting with $\bar{x}_i = 10^{-3}$ at $z = 12$. The different lines of the same type are for MHR (top), minihalo (middle), and MIPS (bottom) recombination. The minihalo (center) lines are shown for two different Monte Carlo runs to illustrate the run to run scatter. The solid line is the fiducial model, the short dashed and dotted lines correspond to the models with only black holes and stars respectively. The heavy dotted line is the ionization fraction for a $\zeta(m) \sim m^{2/3}$ model (eq. 38, similar to FMH05).

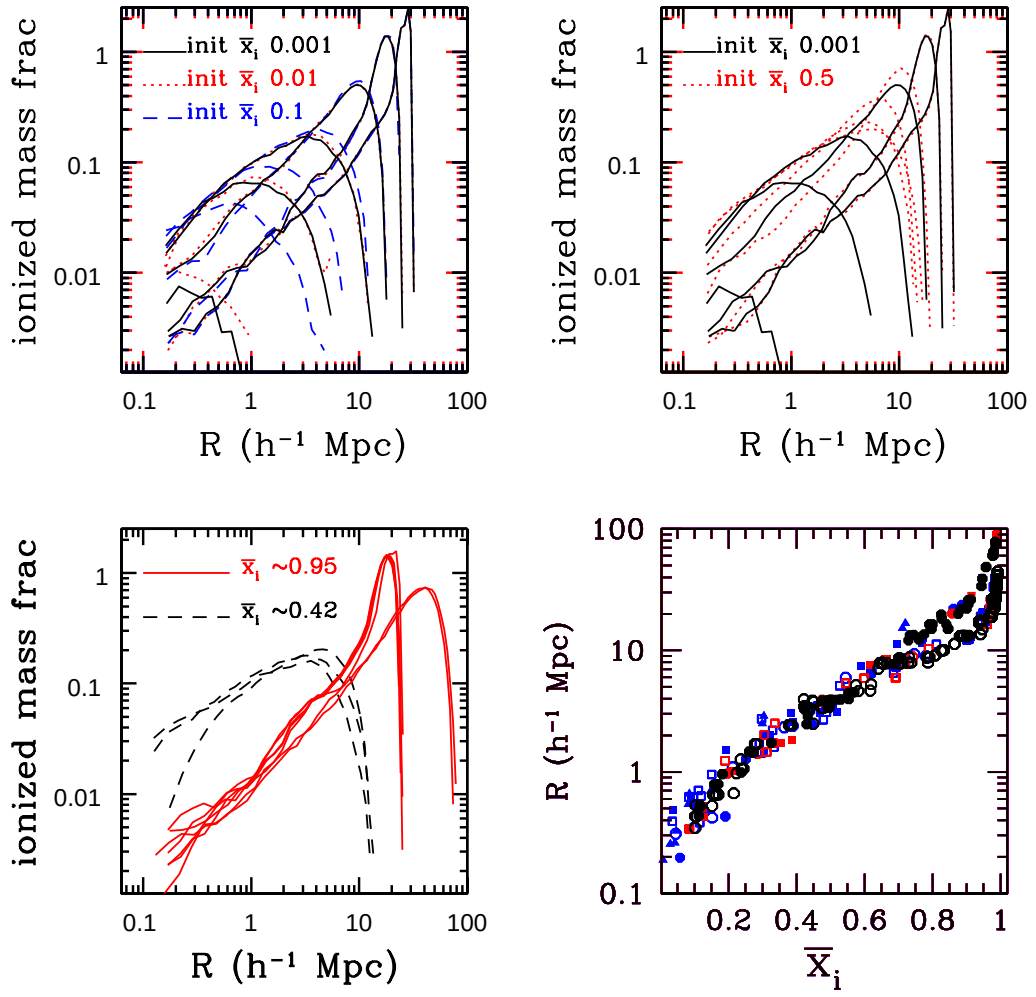

Figure 7: Variations due to different modeling assumptions. Top left and right: initial condition dependence for minihalo recombination. At left, initial ($z = 12$) $\bar{x}_i = 10^{-3}$ (solid),10^{-2} (dots),10^{-1} (dots), for $z = 11.9, 11, 10, 9, 8, 7$. At right initial $z = 12$ $\bar{x}_i = 10^{-3}$ (solid),0.5 (dots), for the same redshifts. Bottom left: distributions for models with $\bar{x}_i \sim 0.42$ (dashed), 0.95 (solid). For low $\bar{x}_i$ the $\ln R$ distributions are similar, irrespective of recombination or other modeling assumptions, for high $\bar{x}_i$ the profile depends strongly on the recombination choice (the rightmost peak is MHR recombination, the peak left of it is minihalo recombination, for several models). Bottom right: R_c as a function of $\bar{x}_i$ is shown for all the models to illustrate trends and model to model scatter. Open symbols are minihalo recombinations. Squares are for $n = 1.05$ models, $f_* f_{esc} \to 4 f_* f_{esc}$, $\Omega_b h^2 = 0.0225$, octagons are for the fiducial model with varied initial conditions, including an initial condition set at $z = 16$, two variations of $m_{0,min}$ 3σ or 3.5σ seed black holes, $\alpha = 2/3$ or $\alpha = 0$, and stars only and 3.5σ black holes only. Filled symbols are MHR (octagon/square) recombinations. Filled triangles are MIPS recombinations, show for the fiducial model and 4 other cases: the variation taking $\alpha = 1$, and the other 3 combinations of 3.5σ or 3σ seed black holes and $m_{0.min} = 0.1m$ or $m(T = 10^4 K)$.

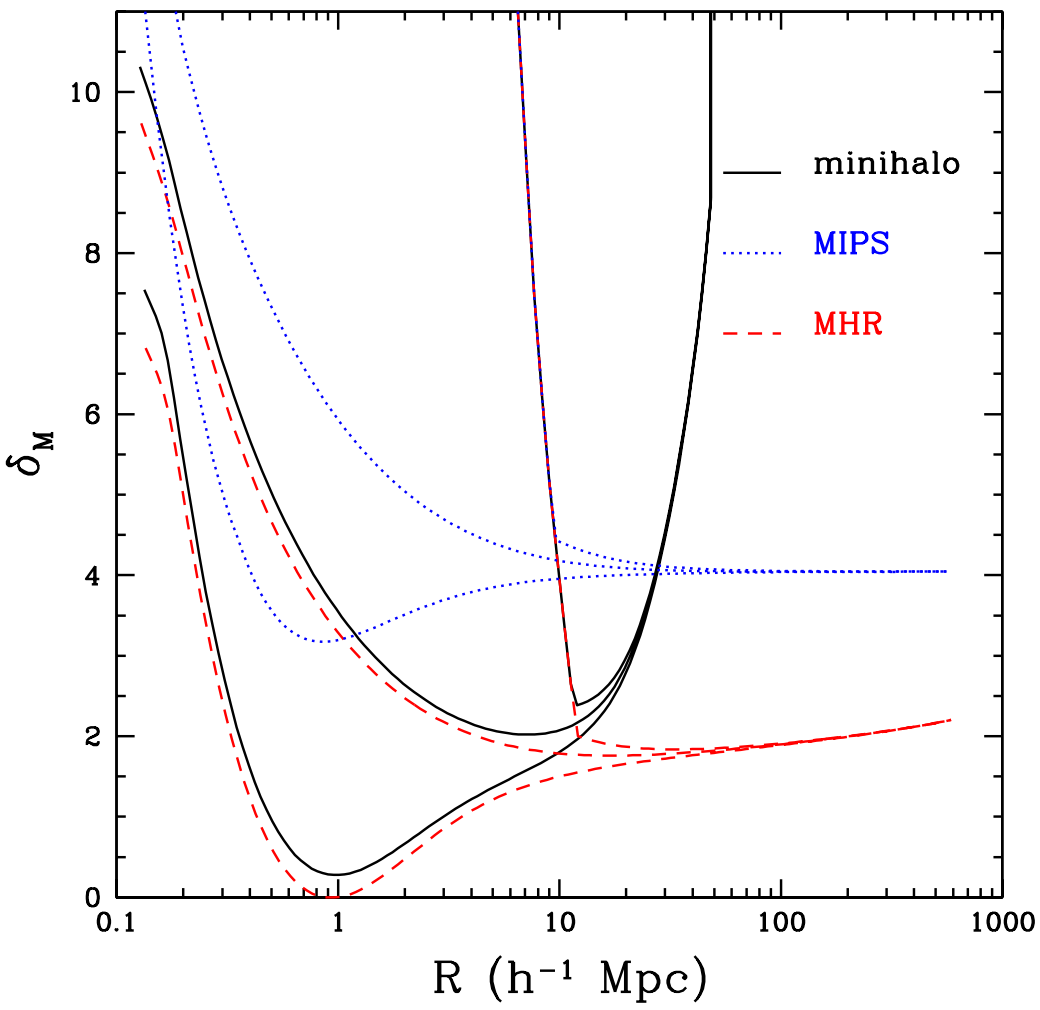

Figure 8: Barriers at $z = 10$ with scatter for the fiducial model. The central line is the mean, lines above and below are 1σ scatter in the time integral of $\zeta_{t,a}(m)$ as using the replacement of equation 41. The solid/dashed/dotted lines are minihalo, MHR, MIPS recombination respectively. The scatter to fewer photons results in a larger bubble size: a larger volume is needed in order to enclose a sufficient numbers of sources.

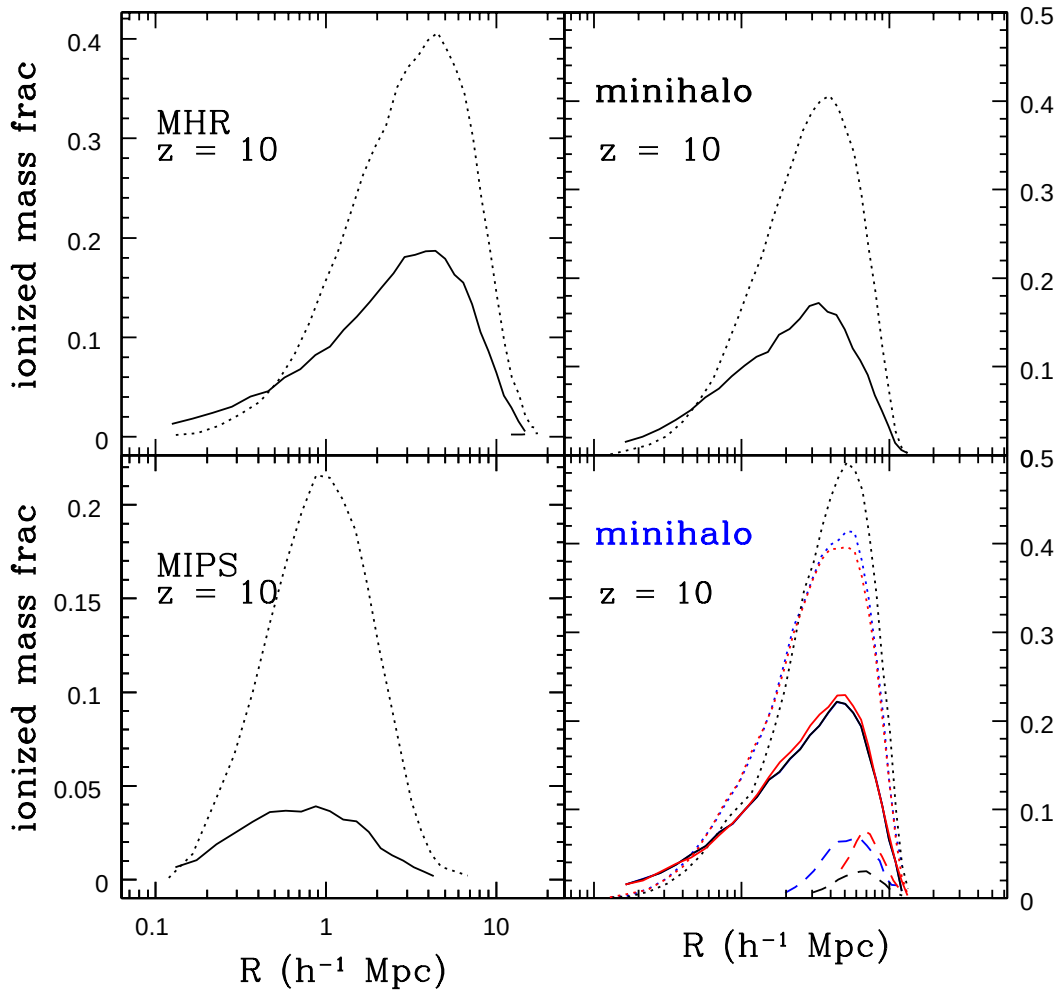

Figure 9: Top left to right and bottom left: Radii at z = 10 and their one sigma scatter up and down for our fiducial case for MHR ($\bar{x}_i = 0.42$), minihalo ($\bar{x}_i = 0.38$), and MIPS ($\bar{x}_i = 0.08$) recombination. Bottom right: 3 estimates for scatter at z=10 for a model with $\bar{x}_i(z = 12) = 0.16$: starting at $z = 16$, starting at $z = 12$ with usual scatter and starting at $z = 12$ doubling the usual scatter. The lines for the scatter to bigger radii starting at z=16 and that starting at z=12 are very similar by $z = 10$. The highest dotted line shows how doubling the scatter translates into a change in the characteristic radii. Solid lines are the mean, dashed lines are scatter to fewer photons, dotted are scatter to more photons. Lines not seen indicate an ionization fraction too small to appear.

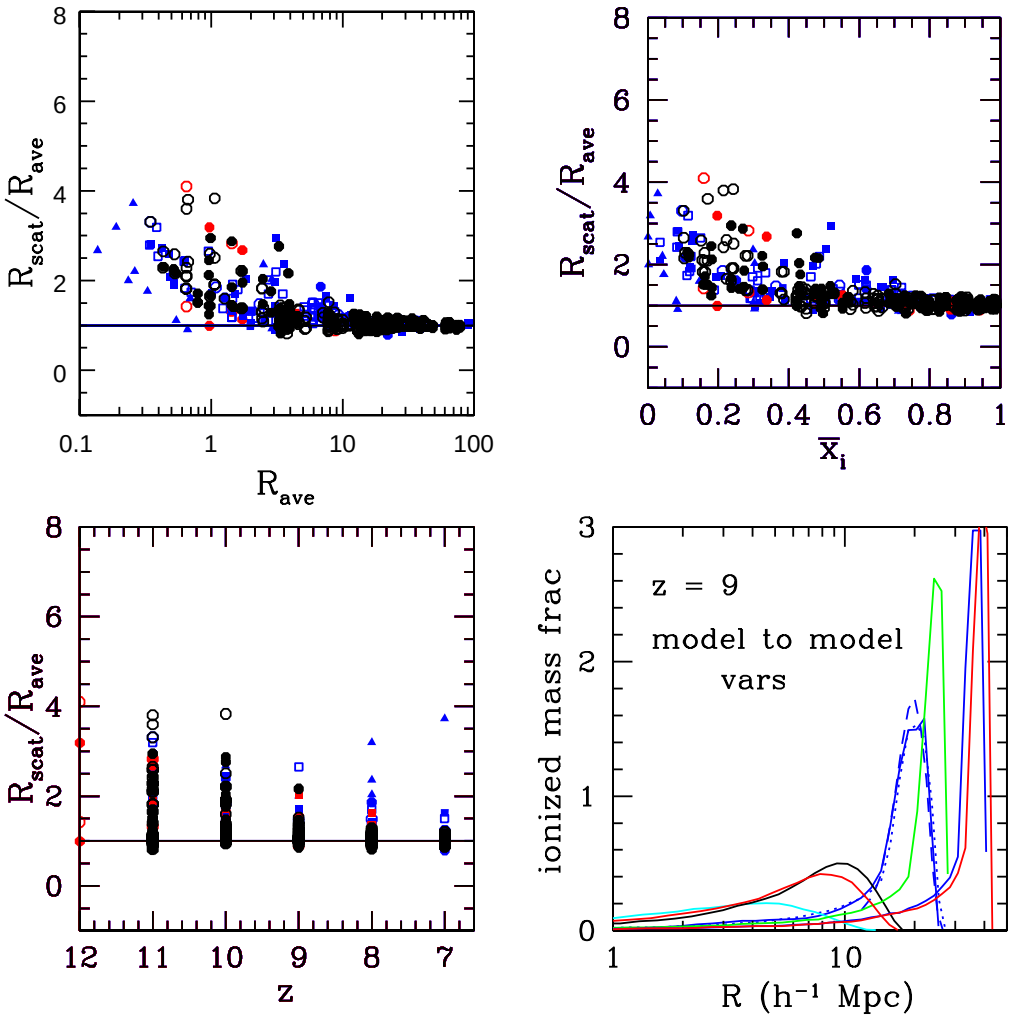

Figure 10: Top left: The ratio R_{scat}/R_{ave} amongst several models as a function of R_{ave}. Top right: The range of the mean value of R_c as a function of $\bar{x}_i$. Bottom left: R_{scat}/R_{ave} as a function of redshift. For all three of these, models with $R_c > 100$ are not shown. Filled symbols are MHR (octagon/square) and MIPS (triangle) recombinations, open symbols are minihalo recombinations, specific models are as in Fig. 7. Bottom right: many different models are shown at $z = 9$. Left to right (smallest to biggest when there is overlap): fixed m_{ref}, $\Omega_b h^2 = 0.0225$, the fiducial model, $n = 1.05, f_* f_{esc} \rightarrow f_* f_{esc} * 4$ (with scatter), 3σ black holes,$\alpha = 0, 3.5\sigma$ black holes, $\alpha = 0, 3\sigma$ black holes.

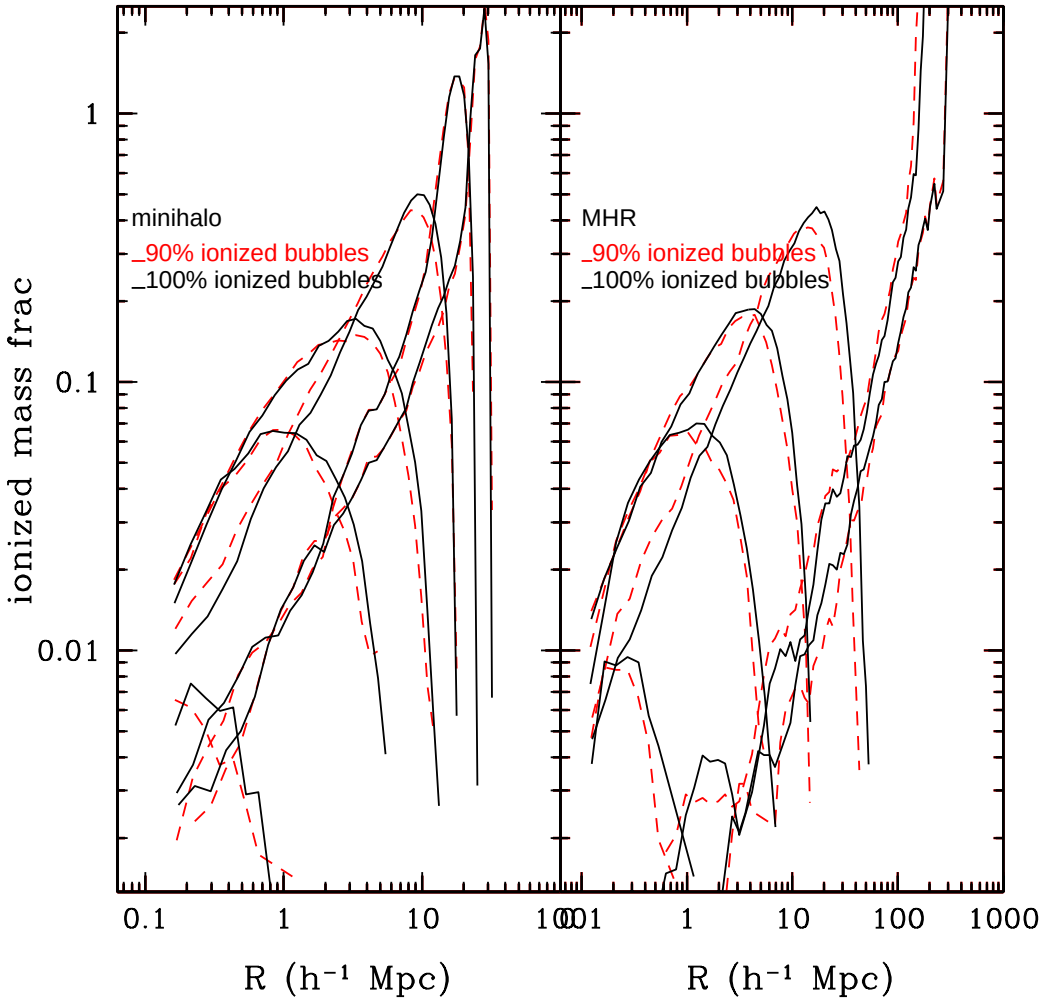

Figure 11: Mass fraction in bubbles as function of radius for bubbles which are 100% ionized (solid) and 90% ionized (dashed) at redshifts 11.9, 11, 10, 9, 8, 7 (lowest to highest curves) for minihalo and MHR recombinations (left and right). The effects of changing between fully ionized to 90% ionized bubbles does not change the distribution as a function of radius that much except at large ionization fraction. Note the radial scale for MHR recombinations is much larger.